

Universiteit
Leiden
The Netherlands

Upconverting nanovesicles for the activation of ruthenium anti-cancer prodrugs with red light

Askes, S.H.C.

Citation
Askes, S. H. C. (2016, November 24). *Upconverting nanovesicles for the activation of ruthenium anti-cancer prodrugs with red light*. Retrieved from https://hdl.handle.net/1887/44378

Version:	Not Applicable (or Unknown)
License:	Licence agreement concerning inclusion of doctoral thesis in the Institutional Repository of the University of Leiden
Downloaded from:	https://hdl.handle.net/1887/44378

Note: To cite this publication please use the final published version (if applicable).

Cover Page



Universiteit Leiden



The handle http://hdl.handle.net/1887/44378 holds various files of this Leiden University dissertation.

Author: Askes, S.H.C.
Title: Converting nanovesicles for the activation of ruthenium anti-cancer prodrugs with red light
Issue Date: 2016-11-24

APPENDIX I: DETERMINATION OF QUANTUM YIELD OF UPCONVERSION

I.1. Experimental setup

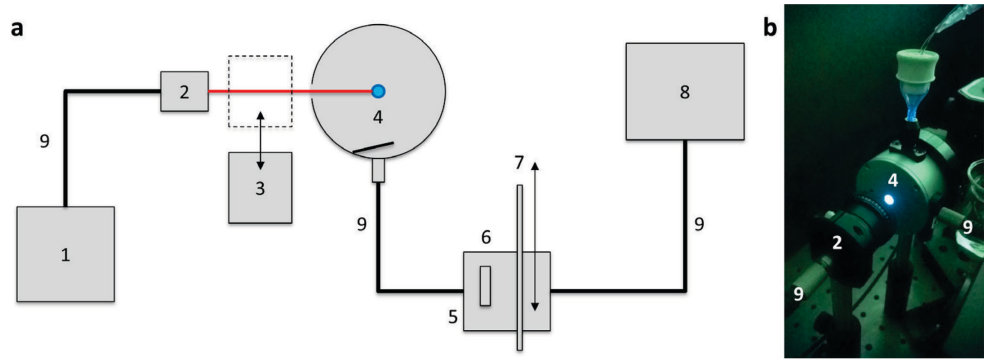


Figure S.I.1. Setup used for absolute quantum yield measurements. a) Schematic representation; (1) 532 nm or 630 nm laser source, (2) collimating lens, 630 nm band pass filter, and mechanical iris – these parts were only used in case of 630 nm excitation (3) power meter adjustable in position, (4) integrating sphere with sample tube in the center, (5) filter holder, (6) notch filter or short pass filter that can be installed or removed, (7) variable neutral density filter that can be installed or removed, (8) CCD spectrometer, (9) optical fibers. b) Picture of the integrating sphere while irradiating a red-to-blue upconverting sample with 630 nm light. A 630 nm notch filter was held in front of the camera to block the red-light scatter. The blue light originates from the upconversion in the sample.

An integrating sphere setup was used for determining the quantum yield of upconversion (Figure S.I.1). For green-to-blue upconversion quantum yield determinations, the excitation source was a 532 nm continuous wave Aries 150 portable DPSS laser from LaserGlow (Toronto, ON, Canada) with a beam diameter of 1.5 mm. For red-to-blue upconversion, the excitation source was a fiber-coupled clinical grade Diomed 630 nm PDT laser. The optical fiber was connected to a collimating lens, after which the light passed a 630 nm band pass filter (Thorlabs, Dachau/Munich, Germany, part no. FB630-10) and a mechanical iris to produce a ca. 2 mm beam. The excitation power was measured using a S310C thermal sensor connected to a PM100USB power meter (Thorlabs). An AvaSphere-30-IRRAD integrating sphere, customized with a sample holder and an extra aperture, and an AvaSpec-ULS2048L StarLine CCD spectrometer were purchased from Avantes (Apeldoorn, The Netherlands). The integrating sphere and spectrometer were calibrated together using a Avalight-HAL-CAL-ISP30 NIST traceable calibration lamp

from Avantes, so that the observed intensities are expressed with the dimension of a photon flux (mol of photons.s^{-1}.nm^{-1}). The filter holder was fabricated by our own mechanical department, and held a NDL-25C-4 variable neutral density filter (Thorlabs), or a NF533-17 notch filter (Thorlabs) in case of excitation with 532 nm light, or an OD4 575 nm short pass filter (Edmund Optics, York, United Kingdom, part no. 84-709) in case of excitation with 630 nm light. The FC-UVxxx-2 (xxx = 200, 400, 600) optical fibers with 200-600 µm diameter were purchased from Avantes and were suitable for the UV-Vis range (200-800 nm). Spectra were recorded with Avasoft software from Avantes and further processed with Microsoft Office Excel 2010 and Origin Pro software.

I.2. Procedure for determining the quantum yield of upconversion

The quantum yield of upconversion (Φ_{uc}) is defined by Equation S.I.1:

$$\Phi_{UC} = \frac{number\ of\ upconverted\ photons}{number\ of\ low\text{-}energy\ photons\ absorbed} = \frac{q_{p-em}}{q_{p-abs}} \qquad \textit{Equation S.I.1}$$

where $q_{p\text{-}em}$ is the emission photon flux of the singlet annihilator species (in photons.s^{-1}) and $q_{p\text{-}abs}$ is the photon flux absorbed by the sensitizer species (in photons.s^{-1}).

Note that for TTA-UC quantum yields, it is common to multiply Φ_{uc} by 2, because TTA-UC intrinsically has a maximum quantum yield of 50% and thus must be scaled to attain a maximum value of 100%. This was only applied in Chapter 3, as it was later realized that this factor is rather confusing.

Φ_{uc} can be calculated by Equation S.I.2:

$$\Phi_{UC} = \frac{\int_{\lambda_1}^{\lambda_2} I_{annihilator}(\lambda)d\lambda}{q_{p-abs}} \qquad \textit{Equation S.I.2}$$

where $I_{annihilator}(\lambda)$ is the spectral luminescence intensity (in photons.s^{-1}.nm^{-1}) of the annihilator species, λ_1 and λ_2 are the low- and high-wavelength

boundaries, respectively, of the upconverted annihilator emission spectrum. $q_{p\text{-}abs}$ is determined by subtracting the spectral light intensity of the excitation source that has passed through the sample ($I_{exc\text{-}sample}$, in photons.s^{-1}.nm^{-1}) from the spectral light intensity of the excitation source that has passed through a blank sample ($I_{exc\text{-}blank}$, in photons.s^{-1}.nm^{-1}), and by integrating over the excitation wavelength range λ_3 to λ_4, see Equation S.I.3. The blank sample resembled the upconverting sample in all ways, except that it did not contain any sensitizer, and thus did not absorb at the excitation wavelength.

$$q_{p-abs} = \int_{\lambda_3}^{\lambda_4} (I_{exc-blank}(\lambda) - I_{exc-sample}(\lambda))d\lambda \qquad \textit{Equation S.I.3}$$

Equation S.I.2 can then be expressed as Equation S.I.4:

$$\Phi_{UC} = \frac{\int_{\lambda_1}^{\lambda_2} I_{annihilator}(\lambda)d\lambda}{\int_{\lambda_3}^{\lambda_4} (I_{exc-blank}(\lambda) - I_{exc-sample}(\lambda))d\lambda} \qquad \textit{Equation S.I.4}$$

The spectrometer and the integrating sphere were calibrated so that the observed intensities are directly proportional to the photon flux, *i.e.* $I(\lambda) \propto [mol\ of\ photons.s^{-1}.nm^{-1}]$. Therefore, integrating these values over the relevant wavelength regions gave directly the flux of photons arriving at the spectrometer.

Because the intensity of the upconverted light is relatively low compared to that of the exciting laser source the absorption and emission of the sample cannot be measured at the same time. In other words, the laser light saturates the spectrometer, which prevents upconversion to be measured. To circumvent this problem, the absorption was measured using a variable neutral density filter with known attenuation (typically $F_{attn} \approx 0.01$, *i.e.*, ~99% attenuation). This filter was placed between the integrating sphere and the spectrometer to measure the absorbed photon flux, whereas it was replaced for the measurement of the upconverted emission by a notch (533 nm) or by an OD4 short pass filter (< 575 nm) to remove the excitation wavelength. Thus, Equation S.I.4 was changed into Equation S.I.5. The attenuation factor F_{attn} was averaged over the wavelength range of the laser (520 – 540 nm or 615 – 645 nm).

Additionally, during the research described in Chapter 4 and Chapter 9 it was realized a correction was necessary for $I_{annihilator}$ to account for the secondary inner-filter effect, *i.e.* reabsorption of the upconverted light. This reabsorption occurred because the samples were relatively concentrated so that enough excitation light was absorbed to have an accurate value of $q_{p\text{-}abs}$. To this end, the upconversion emission spectrum was recorded under highly diluted conditions in the temperature controlled cuvette holder setup (*e.g.* section 4.4.5) and this spectrum was scaled at the second emission peak of the annihilator (*i.e.* 474 nm for perylene and 486 nm for 2,5,8,11-tetra(*tert*-butyl)perylene), which cannot be reabsorbed, to match the photon flux value at 474 nm / 486 nm of $I_{annihilator}$. This corrected spectrum was called $I_{annihilator\text{-}corr}$. *Note that this correction has not been applied for the quantum yield determination in Chapter 3, i.e. for those calculations* $I_{annihilator\text{-}corr} = I_{annihilator}$.

Finally, although at first the notch or short pass filter was assumed to only block the laser signal from reaching the spectrometer, in reality there was a small reduction of transmission for wavelengths situated in the upconversion range as well. This filtering can be corrected when calculating Φ_{uc} by dividing the upconversion luminescence intensity by the transmission curve $T(\lambda)$ of the notch or short pass filter in the wavelength range of the upconverted light. The corrected equation for Φ_{uc} became Equation S.I.5:

$$\Phi_{UC} = \frac{\int_{\lambda_1}^{\lambda_2} \left(\frac{I_{annihilator-corr}(\lambda)}{T(\lambda)} \right) d\lambda}{\int_{\lambda_3}^{\lambda_4} \frac{I_{exc-blank}(\lambda) - I_{exc-sample}(\lambda)}{F_{attn}} d\lambda} \equiv \frac{q_{p-em}}{q_{p-abs}} \qquad \textit{Equation S.I.5}$$

The boundary wavelengths that were used for determining Φ_{uc}, as well as the measured values for $q_{p\text{-}em}$ and $q_{p\text{-}abs}$ at 293 K, are given in Table S.I.1.

Because the integrating sphere setup did not feature temperature control, Φ_{UC} at 310 K was estimated from measuring the upconversion emission under highly diluted conditions in the temperature controlled cuvette holder setup at 293 K and at 310 K (*e.g.* Section 4.4.5) and scaling Φ_{UC} at 293 K with the ratio of the upconversion emission at 293 K and 310 K by using Equation S.I.6:

$$\Phi_{UC}^{310\,K} = \Phi_{UC}^{293\,K} * \frac{\int_{\lambda_1}^{\lambda_2} I_{annihilator}^{310\,K}(\lambda)d\lambda}{\int_{\lambda_1}^{\lambda_2} I_{annihilator}^{293\,K}(\lambda)d\lambda} \qquad \textit{Equation S.I.6}$$

Table S.I.1. Values used throughout this thesis for Φ_{uc} determination at 293 K. See each chapter for the exact sample formulations.

Chapter	Sample	λ_1 (nm)	λ_2 (nm)	λ_3 (nm)	λ_4 (nm)	$q_{p\text{-}em}$ (nmol photon s.s^{-1})	$q_{p\text{-}abs}$ (nmol photon s.s^{-1})	Φ_{uc}
Chapter 3	**L1-2**	390	525	520	545	0.0384	3.32	0.023
	PtOEP & DPA in toluene[a]	390	525	520	545	0.124	4.81	0.051
	L3-4	400	575	615	645	0.0306	11.4	0.0054
	PdTPTBP & perylene in toluene[b]	400	600	615	645	0.0420	7.13	0.012
Chapter 4	**L12**	400	575	615	645	0.705	30.0	0.024
Chapter 9	**P3-1-2**	400	575	615	645	0.0925	45.3	0.0020
	P4-1-2	400	575	615	645	0.103	49.7	0.0021

[a] [PtOEP] = 3.5 μM, [DPA] = 100 μM. [b] [PdTPTBP] = 2.5 μM, [perylene] = 50 μM. PtOEP = platinum(II) octaethylporphyrin, DPA = 9,10-diphenylanthracene, PdTPTBP = palladium (II) tetraphenyltetrabenzoporphyrin

For each measurement, two liposome or polymersome samples were prepared: one blank sample, containing only the annihilator but deprived of sensitizer. Since the concentration of the sensitizer is very small compared to the other sample constituents ([sensitizer] ≤ 0.05 mol%), we assume that removal of the sensitizer from the lipid or polymer mixture did not influence the physical properties of the vesicles (membrane fluidity, scattering properties of the sample, or others). The upconverting sample or the blank sample was loaded into specially designed measurement tubes that were made of a quartz EPR-tube bottom (± 7 cm length) fused to a NS-14 glass connector (± 2 cm length), at the top of which a septum was adapted. The tube fit precisely a hole made in the integrating sphere, and reached the center of the sphere, where it was hit by the excitation laser beam.

In Chapter 3 and Chapter 4, deoxygenation of the sample was performed in a separate ice-cooled, pear-shaped flask, by bubbling the sample with argon for at least 30 minutes with a rate of 1 − 2 mL per second. The degassed sample was then transferred to the measurement tube by cannulation in the strict

absence of oxygen. Degassing in the tube was found to be impossible due to foam formation. In Chapter 9, the samples were 1:1 v/v mixed with a 50 mM Na_2SO_3 solution in PBS to chemically deoxygenate the samples and allow measurements to conveniently take place in air. For these measurements, the final concentrations were [PiB-PEG-Me polymer] = 5.0 mg/mL, [sensitizer] = 5 μM, and [annihilator] = 100 μM.

APPENDIX II: SUPPORTING INFORMATION FOR CHAPTER 3

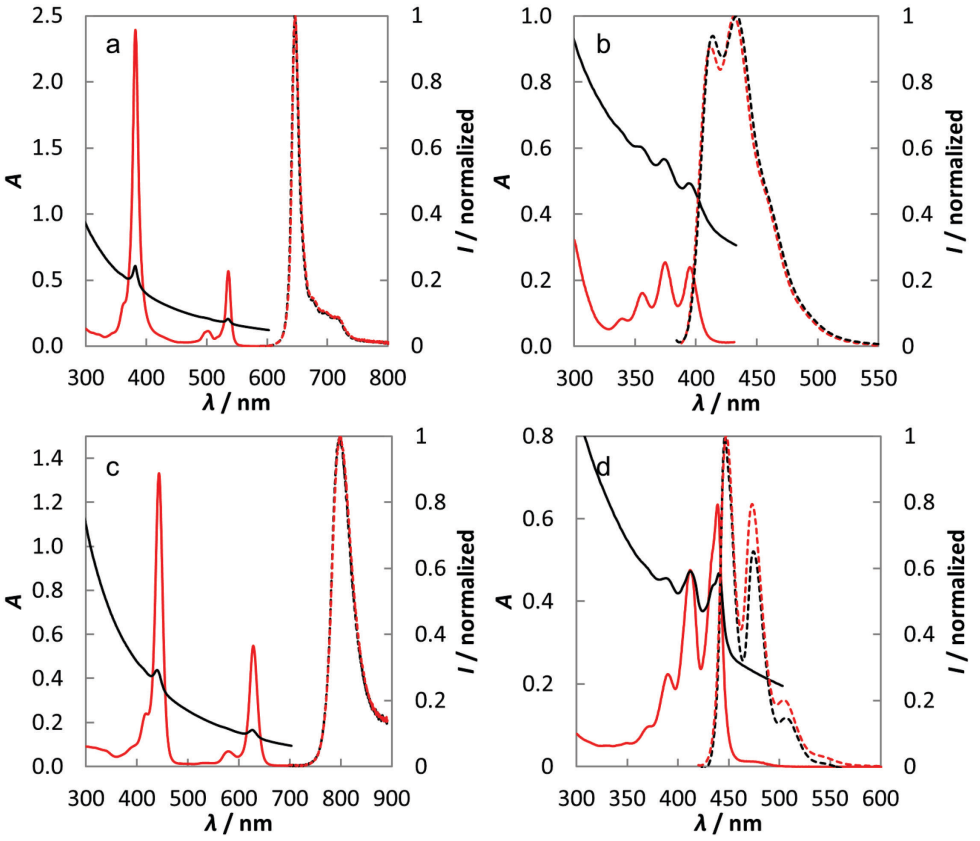


*Figure S.II.1. Absorbance (left axes, solid lines) and normalized emission (right axes, dashed lines) spectra of compounds **1-4** in toluene solution (red) and in liposome samples (black). Liposome samples were diluted 12 times with respect to the formulation given in Table 3.1, to keep absorbance values low enough. Absorbance spectra of liposome samples are uncorrected for scattering. Samples containing compound **1** or **3** were deoxygenated thoroughly before measurement by bubbling the sample with argon for 30 min with a rate of ~2 bubbles per second. All spectra were taken at room temperature. (a) Sample **L1** ([**1**] = 0.3 μM) and **1** in toluene (7 μM). For emission, λ_{exc} = 532 nm. (b) Sample **L2** ([**2**] = 8 μM) and **2** in toluene (20 μM). For emission λ_{exc} = 378 nm. (c) Sample **L3** ([**3**] = 0.2 μM) and **3** in toluene (5 μM). For emission λ_{exc} = 630 nm. (d) Sample **L4** ([**4**] = 4 μM) and **4** in toluene (20 μM). For emission, λ_{exc} = 416 nm.*

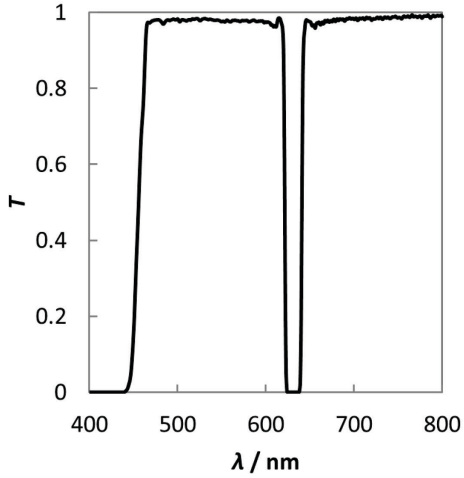


Figure S.II.2. Transmission curve of the 633 nm notch filter used in this work (Thorlabs part no. NF633-25). The low transmission for λ ≤ 450 nm explains the difference between the emission of ***4*** *in Figure S.II.1d and the upconverted emission of* ***4*** *as observed in spectra acquired in upconversion experiments using the 633 nm notch filter (Figure 3.3).*

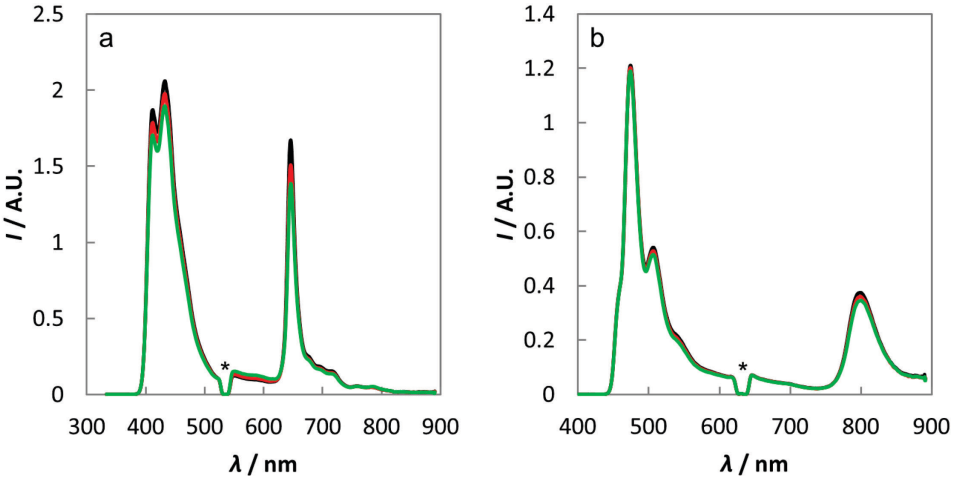


Figure S.II.3. (a) Emission spectra of couple ***1-2*** *([****1****] = 3.5 µM, [****2****] = 100 µM) in toluene at 288 K (black line), 293 K (red line), and 298 K (green line). (b) Emission spectra of couple* ***3-4*** *([****3****] = 2.5 µM, [****4****] = 50 µM) in toluene at 288 K (black line), 293 K (red line), and 298 K (green line). Asterisks indicate excitation wavelength: couple* ***1-2*** *and couple* ***3-4*** *were excited at 532 nm and 630 nm, respectively. Samples were thoroughly deoxygenated before measurement. The excitation power for both samples was 27 mW in a 2.6 mm diameter beam (light intensity: 0.51 W.cm^{-2}).*

APPENDIX III: SUPPORTING INFORMATION FOR CHAPTER 4

III.1. Ru concentration in liposome samples by inductively coupled plasma optical emission spectroscopy

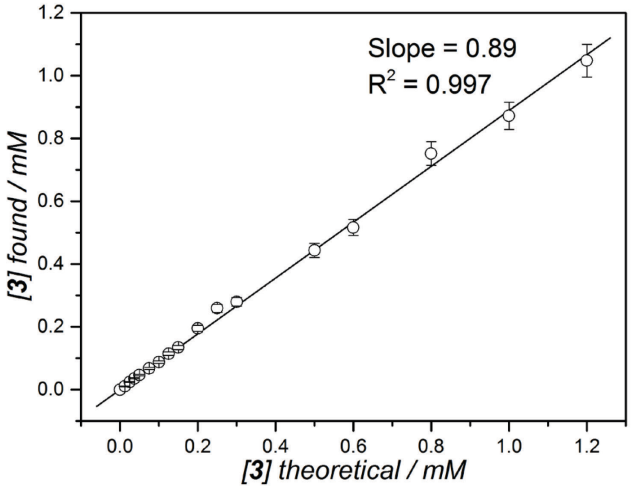


Figure S.III.1. Bulk concentrations of $\mathbf{3}^{2+}$ *experimentally found in PEGylated DMPC liposome samples, determined by inductively coupled plasma optical emission spectroscopy, versus theoretical concentrations. As best fit, a straight line was plotted through the origin with a slope of 0.89 (*R^2 *= 0.997). Error bars represent 5% instrumental error.*

The bulk concentration of $\mathbf{3}^{2+}$ in liposome samples was measured with inductively coupled plasma optical emission spectroscopy (ICP-OES), see Figure S.III.1. From the slope of a linear fit of the measured values plotted *versus* theoretical values it was determined that on average, 89% of the theoretical concentration $\mathbf{3}^{2+}$ was experimentally found. In all experiments when the determined value was too low with respect to the threshold of the ICP-OES machine, an extrapolated value was used from the theoretical concentration multiplied by 0.89.

III.2. Differential scanning calorimetry

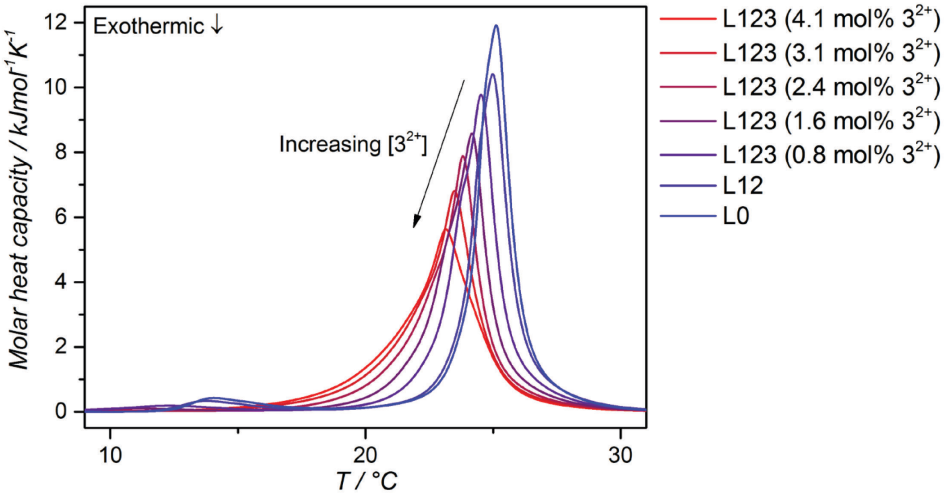


*Figure S.III.2. Differential scanning calorimetry thermograms (in heating mode) for PEGylated (4 mol%) DMPC liposomes without any chromophores (**L0**), with the TTA-UC dye couple (**L12**), and with the TTA-UC dye couple and various amounts of **3**$^{2+}$ added (**L123**). Reported molar percentages of **3**$^{2+}$ are based on ICP-OES measurements (see Chapter 4). Measurements were performed with a scanning rate of 1 K.min^{-1} at 3 atm. pressure.*

*Table S.III.1. Differential scanning calorimetry data for PEGylated (4 mol%) DMPC liposomes without any chromophores (**L0**), with the TTA-UC dye couple (**L12**), and with the TTA-UC dye couple and various amounts of **3**$^{2+}$ added (**L123**) , with T_m (in °C) as the main transition temperature and ΔH (in kJ.mol^{-1}) as the molar change in enthalpy when heating from 10 to 35 °C. Reported molar percentages of **3**$^{2+}$ are based on ICP-OES measurements (see Chapter 4). Measurements were performed with a scanning rate of 1 K.min^{-1} at 3 atm. pressure.*

Sample	**3^{2+} molar percentage**	***T*$_m$ (°C)**	**Δ*H* (kJ.mol^{-1})**
L0		25.1	25.1
L12		25.0	23.1
L123	0.8	24.5	23.8
L123	1.6	24.2	22.4
L123	2.4	23.8	21.6
L123	3.1	23.5	21.7
L123	4.1	23.2	21.1

III.3. Photodissociation experiments using red light

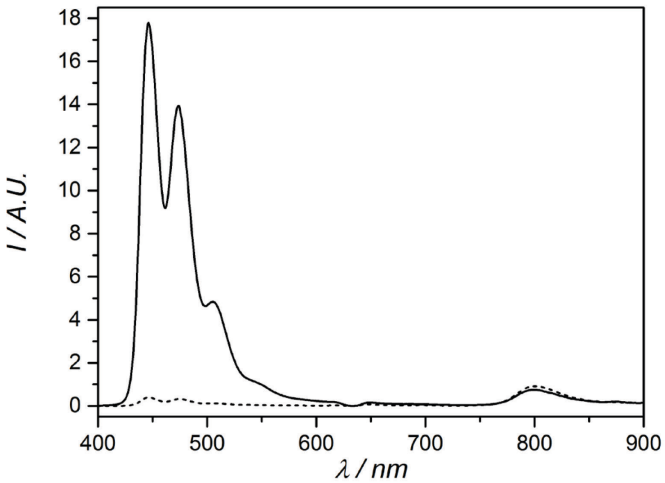


*Figure S.III.3. Luminescence emission spectrum of **L12** (black) and **L123** with 3.3 mol% **3**$^{2+}$ at t = 0 of the irradiation experiment using red light (dashed). λ_{exc} = 630 nm. Irradiation conditions: power 120 mW, beam diameter 4 mm, intensity 0.95 W.cm^{-2}, T = 310 K, sample volume 1.5 ml. The liposome dispersion was diluted prior to measurement so that [**2**] = 2.5 µM and [**1**] = 0.25 µM, and in the case of **L123**, the concentration of **3**$^{2+}$ = 18 µM.*

III.4. Lifetime studies with time-correlated single photon counting and transient absorption spectroscopy

III.4.1. Analysis of time-correlated single photon counting data

Fluorescence lifetime measurements were performed using time-correlated single photon counting (TCSPC). The obtained histograms were fitted with Origin Pro software as the sum of single exponential decays, as described by Equation S.III.1:

$$I(t) = \sum_i A_i e^{\frac{t}{\tau_i}} \qquad \textit{Equation S.III.1}$$

where t is time, *I(t)* is the time-dependent observed emission intensity (photon counts), A_i is the decay amplitude, and τ_i is the decay constant. For each sample, fitting with a single exponential decay curve did not give satisfactory fits. In the case of liposomes **L2**, this is attributed to the molecules being dissolved in a heterogeneous system (*e.g.* liposomes), and a small degree of self-energy transfer (homo-transfer) due to clustering of **2** in the membrane.[1] In the case of **L23** or **L123**, the occurrence of energy transfer results in a multitude of donor excited state lifetimes, *i.e.* multi-exponential decays. To achieve a single lifetime value, required for further data processing, it was therefore necessary to use amplitude weighted average lifetimes (τ), as calculated by Equation S.III.2:

$$\tau = \frac{\sum_i A_i \tau_i}{\sum_i A_i} \qquad \textit{Equation S.III.2}$$

III.4.2. Time-correlated single photon counting data

*Table S.III.2. Fitting parameters to various decay functions for the fluorescence lifetime (in ns) of compound 2, as measured with TCSPC at 293 K (λ_{exc} = 440 nm, and λ_{em} = 474 nm), in PEGylated DMPC liposomes with a fixed amount (0.5 mol%) of **2** while varying the molar percentage of **3**$^{2+}$ from 0 to 6%, as well as the calculated parameters τ as the amplitude averaged lifetime calculated from τ_1, A_1, τ_2, A_2, τ_3, and A_3 by Equation S.III.2, and E_{ET} as the efficiency of energy transfer calculated from Equation S.III.6. Goodness of fit expressed as R^2 values. The bulk concentration of 3^{2+} was determined by ICP-OES. Bulk concentration of DMPC, DSPE-PEG-2000, and compound **2** were 0.20 mM, 8 µM, and 1 µM, respectively.*

Decay function	**Concentration of 3^{2+} in the membrane in mol%**					
	0.0%	0.2%	0.5%	0.7%	0.9%	1.7%
Multi-exponential						
τ_1 (A_1 in %)	6.49 ± 0.01 (93%)	5.82 ± 0.01 (77%)	5.37 ± 0.01 (83%)	5.10 ± 0.13 (44%)	4.56 ± 0.08 (36%)	2.43 ± 0.03 (37%)
τ_2 (A_2 in %)	1.58 ± 0.06 (7%)	1.64 ± 0.02 (23%)	1.30 ± 0.02 (17%)	2.09 ± 0.16 (38%)	1.79 ± 0.08 (42%)	0.79 ± 0.05 (40%)
τ_3 (A_3 in %)				0.63 ± 0.04 (19%)	0.54 ± 0.03 (23%)	0.30 ± 0.03 (23%)
τ	6.17 ± 0.01	4.85 ± 0.01	4.67 ± 0.01	3.14 ± 0.08	2.50 ± 0.05	1.29 ± 0.02
R^2	0.9997	0.9996	0.9996	0.9996	0.9995	0.9994
E_{ET}	0%	21%	24%	49%	60%	79%
Förster 3D model						
γ	0.00 ± 0.00	0.23 ± 0.00	0.28 ± 0.00	0.74 ± 0.01	1.044 ± 0.01	1.82 ± 0.01
R^2	0.9995	0.9996	0.9996	0.9995	0.9995	0.999

Decay function	**Concentration of 3^{2+} in the membrane in mol%**				
	2.1%	2.4%	3.5%	5.0%	5.6%
Multi-exponential					
τ_1 (A_1 in %)	2.85 ± 0.08 (21%)	3.35 ± 0.19 (18%)	2.12 ± 0.18 (19%)		
τ_2 (A_2 in %)	0.98 ± 0.06 (42%)	1.21 ± 0.08 (41%)	0.85 ± 0.14 (33%)	1.20 ± 0.01 (24%)	0.96 ± 0.01 (41%)
τ_3 (A_3 in %)	0.32 ± 0.02 (36%)	0.37 ± 0.01 (41%)	0.33 ± 0.02 (48%)	0.31 ± 0.00 (76%)	0.29 ± 0.01 (59%)
τ	1.14 ± 0.03	1.25 ± 0.05	0.85 ± 0.06	0.53 ± 0.00	0.57 ± 0.01
R^2	0.9992	0.9993	0.9992	0.9991	0.9992
E_{ET}	82%	80%	86%	91%	91%
Förster 3D model					
γ	2.04 ± 0.01	1.93 ± 0.01	2.67 ± 0.02	3.99 ± 0.08	3.84 ± 0.08
R^2	0.9992	0.9993	0.9991	0.9991	0.9991

*Table S.III.3. Fitting parameters to various decay functions for the fluorescence lifetime (in ns) of compound **2**, as measured with TCSPC at 310 K (λ_{exc} = 440 nm, and λ_{em} = 474 nm), in PEGylated DMPC liposomes with a fixed amount (0.5 mol%) of **2** while varying the molar percentage of **3**$^{2+}$ from 0 to 6%, as well as the calculated parameters τ as the amplitude averaged lifetime calculated from τ_1, A_1, τ_2, A_2, τ_3, and A_3 by Equation S.III.2, and E_{ET} as the efficiency of energy transfer calculated from Equation S.III.6. Goodness of fit expressed as R^2 values. The bulk concentration of **3**$^{2+}$ was determined by ICP-OES. Bulk concentration of DMPC, DSPE-PEG-2000, and compound **2** were 0.20 mM, 8 µM, and 1 µM, respectively.*

Decay function	**Concentration of 3^{2+} in the membrane in mol%**					
	0.0%	0.2%	0.5%	0.7%	0.9%	1.7%
Multi-exponential						
τ_1 (A_1 in %)	5.94 ± 0.01 (94%)	5.33 ± 0.01 (80%)	4.79 ± 0.01 (77%)	4.01 ± 0.03 (63%)	4.06 ± 0.11 (36%)	
τ_2 (A_2 in %)	2.01 ± 0.10 (6%)	1.72 ± 0.03 (20%)	1.35 ± 0.02 (23%)	1.38 ± 0.10 (29%)	1.86 ± 0.13 (41%)	1.85 ± 0.01 (45%)
τ_3 (A_3 in %)				0.49 ± 0.09 (9%)	0.64 ± 0.03 (23%)	0.54 ± 0.00 (55%)
τ	5.69 ± 0.01	4.60 ± 0.01	4.00 ± 0.01	2.96 ± 0.03	2.37 ± 0.07	1.14 ± 0.00
R^2	0.9997	0.9997	0.9996	0.9996	0.9996	0.9995
E_{ET}	0%	19%	30%	52%	58%	80%
Förster 3D model						
γ	0.00 ± 0.01	0.22 ± 0.00	0.36 ± 0.00	0.74 ± 0.01	1.15 ± 0.01	2.25 ± 0.02
R^2	0.9996	0.9997	0.9996	0.9996	0.9996	0.9994

Decay function	**Concentration of 3^{2+} in the membrane in mol%**				
	2.1%	2.4%	3.5%	5.0%	5.6%
Multi-exponential					
τ_1 (A_1 in %)	2.61 ± 0.20 (7%)				
τ_2 (A_2 in %)	1.07 ± 0.08 (32%)	1.53 ± 0.01 (38%)	0.84 ± 0.01 (29%)	0.66 ± 0.01 (13%)	0.72 ± 0.01 (17%)
τ_3 (A_3 in %)	0.40 ± 0.02 (61%)	0.43 ± 0.00 (62%)	0.30 ± 0.00 (71%)	0.23 ± 0.00 (87%)	0.26 ± 0.00 (83%)
τ	0.77 ± 0.03	0.84 ± 0.00	0.45 ± 0.00	0.29 ± 0.00	0.34 ± 0.00
R^2	0.9993	0.9993	0.9994	0.9985	0.9990
E_{ET}	87%	85%	92%	95%	94%
Förster 3D model					
γ	2.86 ± 0.02	2.75 ± 0.01	5.49 ± 0.09	8.46 ± 0.19	7.25 ± 0.14
R^2	0.9993	0.9992	0.9993	0.9982	0.9989

III.4.3. Analysis of transient absorption data

Data from transient absorption (TA) spectroscopy was fitted using the software package Glotaran, with which the user can conveniently analyze TA data and correct for experimental artefacts. The software features global fitting, with which different components that contribute to the data can be untangled and represented as separate datasets.[2] Each component i in the observed time-dependent transient absorption spectrum $\Delta OD(t,\lambda)$ is described with a non-normalized Decay-Associated transient absorption Spectrum $DAS_i(\lambda)$ and a single exponential decay function with decay constant τ_i, see Equation S.III.3:

$$\Delta OD(t,\lambda) = \sum_i DAS_i(\lambda) * e^{\frac{t}{\tau_i}} \qquad \textit{Equation S.III.3}$$

In the case of multi-exponential behavior of one of the species (*i.e.* **2** in presence of $\mathbf{3}^{2+}$), multiple components were identified with different τ_i, but with identical $DAS_i(\lambda)$. The amplitude averaged lifetime (τ) was then calculated using Equation S.III.4:

$$\tau = \frac{\sum_i B_i \tau_i}{\sum_i B_i} \qquad \textit{Equation S.III.4}$$

in which B_i represents the relative amplitude of DAS_i. For measurements on liposomes **L2** and **L23**, *i.e.* experiments that were meant to probe the lifetime of **2**, B_i was calculated from the average *DAS* value at 695 − 705 nm, at which **2** has a very strong transient peak, while the influence of $\mathbf{3}^{2+}$ is negligible (see below). For measurements on liposomes with only $\mathbf{3}^{2+}$ (*i.e.* **L3** liposomes), A_i was calculated from the average *DAS* value from 445 − 455 nm, where the transient absorption of $\mathbf{3}^{2+}$ is strongest (see below).

III.4.4. Transient absorption data

*Table S.III.4. Fitting parameters to various decay functions for the excited state lifetime (in ns) of compound **2**, as measured with TA spectroscopy at 293 K (λ_{exc} = 400 nm), in PEGylated DMPC liposomes with a fixed amount (0.5 mol%) of **2** while varying the molar percentage of **3**$^{2+}$ from 0 to 3%, as well as the calculated parameters τ as the amplitude averaged lifetime calculated from τ_3, B_3, τ_4, and B_4 by Equation S.III.4, and E_{ET} as the efficiency of energy transfer calculated from Equation S.III.6. Goodness of fit expressed as R^2 values. Bulk concentration of DMPC, DSPE-PEG-2000, and compound **2** were 20 mM, 0.8 mM, and 0.1 mM, respectively. All experimental details can be found in the experimental section.*

Kinetic model	**Concentration of 3^{2+} in the membrane in mol%**					
	0	0.4%	0.8%	1.7%	2.5%	3.3%
Multi-exponential (GLOTARAN)						
τ_1	0.10E−3 ± 0.00E−3	0.01E−3 ± 0.00E−3	0.11E−3 ± 0.00E−3	0.02E−3 ± 0.00E−3	0.09E−3 ± 0.00E−3	0.07E−3 ± 0.00E−3
τ_2	8.3E−3 ± 0.1E−3	8.9E−3 ± 0.09E−3	9.2E−3 ± 0.13E−3	9.1E−3 ± 0.14E−3	9.9E−3 ± 0.17E−3	5.5E−3 ± 0.11E−3
τ_3 (B_3 in %)	2.30 ± 0.12 (22.1%)	0.45 ± 0.00 (27.0%)	0.26 ± 0.00 (41.7%)	0.19 ± 0.00 (49.1%)	0.11 ± 0.00 (57.6%)	0.07 ± 0.00 (55.3%)
τ_4 (B_4 in %)	7.05 ± 0.12 (77.9%)	3.99 ± 0.02 (73.0%)	2.43 ± 0.01 (58.3%)	1.85 ± 0.01 (50.1%)	0.79 ± 0.01 (42.4%)	0.56 ± 0.00 (44.7%)
τ_5	118 ± 34	629 ± 78	916 ± 161	6380 ± 4160	1850 ± 359	613 ± 79
τ	6.00 ± 0.10	3.03 ± 0.02	1.52 ± 0.01	1.04 ± 0.01	0.40 ± 0.00	0.29 ± 0.00
E_{ET}	0%	49.5%	74.7%	82.7%	93.3%	95.1%
Förster 3D model						
γ	0.02 ± 0.02	0.43 ± 0.02	1.00 ± 0.06	1.35 ± 0.05	2.43 ± 0.07	2.99 ± 0.09
R^2	0.9974	0.9991	0.9959	0.9975	0.9968	0.9969

III.4.5. Transient absorption in liposomes L2

The transient absorption spectrum of PEGylated DMPC liposomes bearing 0.5 mol% **2** (liposomes **L2**), 1.0 ns after a 400 nm excitation pulse, is displayed in Figure S.III.4. The spectrum closely matches literature reports for perylene in cyclohexane, and features negative signals from 430 to 550 nm, due to ground state bleach and stimulated emission, and a strong positive band centered at 700 nm, due to excited state absorption as the result of an S_1-S_n transition.[3] The transient absorption data was analyzed with Glotaran and was best-fitted using 5 single-exponential decay functions (Table S.III.4). The fastest decay component (τ_1 = 0.1 ps) is attributed to coherent artefacts due to spatial and temporal overlap of the pump and probe pulses around t = 0. The second decay component (τ_2 = 8.3 ps) is attributed to vibrational relaxation of compound **2** and/or solvent relaxation of the phospholipid matrix. A component with a very long lifetime (τ_5 > 100 ns) and almost negligible amplitude is attributed to either triplet state and/or excimer absorption. The nanosecond scale components with τ_3 = 2.3 and τ_4 = 7.1 ns have identical

spectra, which indicates that they originate from the same species. In this case, τ_1, τ_2, and τ_5 were not taken into account for calculating τ by Equation S.III.4, so that $\tau = \tau_{34}$ = 6.00 ± 0.10 ns, which corresponds to literature values of the excited state lifetime of **2**.[1, 3]

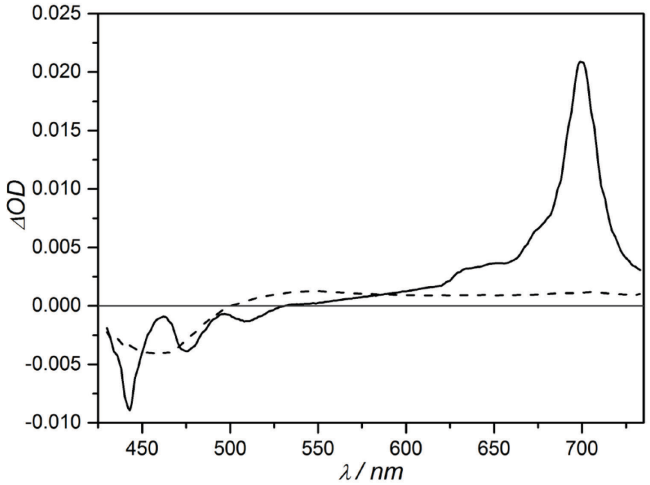


*Figure S.III.4. Transient absorption spectra at 293 K of PEGylated DMPC liposomes with either 0.5 mol% 2 (liposomes **L2**, solid line), 1.0 ns after the excitation pulse, and 3.3 mol% 3^{2+} (liposomes **L3**, dashed line), 1.0 ps after the excitation pulse. Both samples were excited with 400 nm light (20-60 nJ/pulse, 1 kHz repetition rate). Bulk DMPC concentration: 20 mM.*

III.4.6. Transient absorption in liposomes L3

Next, the transient absorption of liposomes with 3.3 mol% of $\mathbf{3}^{2+}$ (liposomes **L3**) was evaluated. It was confirmed with UV-VIS spectroscopy before and after the experiment that negligible photodissociation occurred during the time-resolved spectroscopic analysis. The maximum amount of photodissociation, expressed as the total amount of mol $\mathbf{4}^{2+}$, can be estimated from the photon flux at 400 nm (Φ_{400} = 30 µW, *i.e.* = 1.0 x 10^{-10} einstein.s^{-1}), measurement time (≤ 7200 s), quantum yield of photodissociation (0.52%),[4] and chance of absorption (A_{400} ≤ 0.60), see Equation S.III.5:

$$n_{\mathbf{4}} = (1 - 10^{-A})\Phi_{400}\Phi_{Ru}t \qquad \textit{Equation S.III.5}$$

The value of n_4 for these experiments is ≤ 2.8 x 10^{-9} mol. With a sample volume of 200 µL and a $\mathbf{3}^{2+}$ concentration of 0.71 mM (as determined by ICP-OES),

n_3 = 1.4 x 10^{-7} mol. The maximum amount of photodissociation reaction triggered during the measurement is therefore 2%.

Figure S.III.4 shows the transient absorption spectrum of liposomes **L3** 1.0 ps after the excitation pulse at 400 nm. A negative band ranging from 400 to 500 nm and a weaker positive band from 500 nm onwards are observed. The negative band from 400 to 500 nm coincides with the region of the MLCT absorption band in the steady state absorption spectrum (Figure 1c). Thus this band can be attributed to ground-state bleaching of the ruthenium complex. The broad positive band for λ > 500 nm are attributed to the ^{3}MLCT excited state absorption, as the ^{1}MLCT to ^{3}MLCT intersystem crossing is known to be extremely fast (300 fs time scale).[5] The time evolution of the transient spectrum was best fitted with Glotaran using a model with two exponential decay curves using Glotaran. Two DAS were identified with identical spectra and with lifetimes of 0.17 (53%) and 0.92 ns (47%), hence the average ^{3}MLCT lifetime τ_{Ru} has a value of 0.52 ns.

III.4.7. Transient absorption in liposomes L23

For liposomes **L23**, *i.e.* samples containing both **2** and a varying amount of $\mathbf{3}^{2+}$, the time-dependent absorption data was consistently fitted using 5 single exponential decays, similar to as discussed above (Table S.III.4). Each time, it was most satisfactory to fit the decays in the nanosecond regime with a bi-exponential decay. The decay associated spectra for these two components consistently featured the transient spectral characteristics of compound **2**. For calculation of τ with Equation S.III.4, τ_1, τ_2, and τ_5 were irrelevant, so that the reported τ for liposomes **L23** is each time the average of τ_3 and τ_4, *i.e.* $\tau = \tau_{34}$. The results of these experiments are discussed in the main text.

III.5. Analysis and quantification of non-radiative energy transfer

III.5.1. Calculation of energy transfer efficiency E_{ET}

For liposomes **L23**, the energy transfer efficiency (E_{ET}) values were calculated by Equation S.III.6:

$$E_{ET} = 1 - \frac{\tau}{\tau_0} = 1 - \frac{I}{I_0}$$ *Equation S.III.6*

where τ and τ_0 are the amplitude-weighted averages of the excited state lifetime of compound **2** in presence and absence of $\mathbf{3}^{2+}$, respectively, and I and I_0 are the integrated fluorescence intensity of compound **2** in presence and absence of $\mathbf{3}^{2+}$, respectively.[6] Stern-Volmer kinetics are generally applied to photochemical quenching based on collisional quenching, but are to known to may be applicable to FRET systems as well.[7] By rewriting the classical Stern-Volmer equation, see Equation S.III.7,

$$\frac{\tau_0}{\tau} = 1 + K_{SV}[\mathbf{3}] = 1 + k_{SV}\tau_0[\mathbf{3}]$$ *Equation S.III.7*

an expression for E_{ET} is obtained, see Equation S.III.8:

$$E_{ET} = 1 - \frac{1}{1 + K_{SV}[\mathbf{3}]} = \frac{K_{SV}[\mathbf{3}]}{1 + K_{SV}[\mathbf{3}]}$$ *Equation S.III.8*

where K_{SV} is the Stern-Volmer quenching constant (in $L.mol^{-1}$), k_{SV} is the Stern-Volmer rate of quenching ($L.mol^{-1}.s^{-1}$), τ_0 is the lifetime of the energy donor without any quencher present, and [**3**] is the bulk concentration of $\mathbf{3}^{2+}$. However, the volume in which the quenching occurs is much smaller than the sample volume, because both compound **2** and $\mathbf{3}^{2+}$ are only located within the membrane. Therefore, [**3**] was substituted with $[\mathbf{3}]_{local}$, *i.e.* the local concentration of $\mathbf{3}^{2+}$ at the membrane, which is defined by Equation S.III.9:

$$[\mathbf{3}]_{local} = \frac{n_3}{n_{DMPC}V_M} = \frac{x_3}{V_M}$$ *Equation S.III.9*

where n_3 is the number of mol $\mathbf{3}^{2+}$, as calculated by ICP-OES, n_{DMPC} is the number of mol DMPC, V_M is the molar volume of DMPC in lipid bilayers at 293 K (V_M = 0.637 $L.mol^{-1}$),[8] and x_3 is the mol fraction of $\mathbf{3}^{2+}$ in the lipid bilayer. To simplify, we did not account for the volume of DSPE-PEG-2000, **2**, and $\mathbf{3}^{2+}$, because no data was available, and we did not account for the fact that $\mathbf{3}^{2+}$ occupies a volume outside the lipid bilayer as well. Under these assumptions,

K_{SV} was found to be 0.32 L.mol^{-1}. With τ_0 = 6.2 ns, the value of k_{SV} is 5.2 x 10^7 L.mol^{-1}.s^{-1}.

III.5.2. Calculating the theoretical R_0 distance

One of the prerequisites for FRET is to have a good spectral overlap between the donor emission spectrum and acceptor absorption spectrum, as given by the overlap integral J_{DA} (in M^{-1}.cm^{-1}.nm^4) in Equation S.III.10,

$$J_{DA} = \int_0^\infty F_D(\lambda)\varepsilon_A(\lambda)\lambda^4 d\lambda \qquad \textit{Equation S.III.10}$$

where $F_D(\lambda)$ is the area-normalized donor emission spectrum and $\varepsilon_A(\lambda)$ is the molar absorption spectrum of the acceptor (in L.mol^{-1}.cm^{-1}). J_{DA} = 2.8 x 10^{14} nm^4.M^{-1}.cm^{-1} for **2** as FRET-donor and **3**$^{2+}$ as FRET-acceptor (see Figure 1c). From J_{DA}, the relative orientation factor κ, the refractive index of the medium n (1.334 for PBS buffer), and the fluorescence quantum yield of the donor φ_D, the Förster distance R_0 (in Å) can be calculated, for which half the donor molecules decay by FRET, according to Equation S.III.11 below.[6] Assuming $\kappa^2 = 2/3$ and using φ_D = 0.94 in cyclohexane,[9] R_0 was predicted to be 41 Å.

$$R_0 = 0.211 \times (\kappa^2 n^{-4} \phi_D J_{DA})^{\frac{1}{6}} \qquad \textit{Equation S.III.11}$$

III.5.3. Fitting lifetime data with a Förster decay model

Besides the use of multi-exponential decays to calculate FRET efficiencies and Stern-Volmer parameters, the time-correlated single photon counting data and transient absorption spectroscopy data were also analyzed using a Förster decay model to derive different system parameters. This model has been used before for the analysis of energy transfer from perylene to various transition metal ions in DPPC vesicles.[1, 10] For TCSPC data, Equation S.III.12 was used:

$$I(t) = I_0 e^{-\frac{t}{\tau_0} - 2\gamma\left(\frac{t}{\tau_0}\right)^{1/d}}$$ *Equation S.III.12*

where $I(t)$ is the time-dependent fluorescence intensity, I_0 is the fluorescence intensity directly after excitation, τ_0 is the FRET donor lifetime in absence [1, 10]of the FRET acceptor, d is the dimensionality of the system (d = 2 and d = 3 for quenching in two and three dimensions, respectively), and γ is defined as $[\mathbf{3}]/C_0$, with [**3**] the bulk concentration $\mathbf{3}^{2+}$ (in M) and C_0 the critical acceptor concentration for energy transfer (in M), which is the acceptor concentration needed for 72% energy transfer.[6] In this work, the lifetime data acquired from TCSPC were indeed fitted using the Förster decay model, see Table S.III.2-Table S.III.3. For the fitting, τ_0 was fixed at 6.2 ns. Figure S.III.5 shows a fit of the three-dimensional model (d = 3) on lifetime decay data from TCSPC at 293 K acquired from a liposome sample (**L23**) with 0.5 mol% **2** and 0.9 mol% $\mathbf{3}^{2+}$.

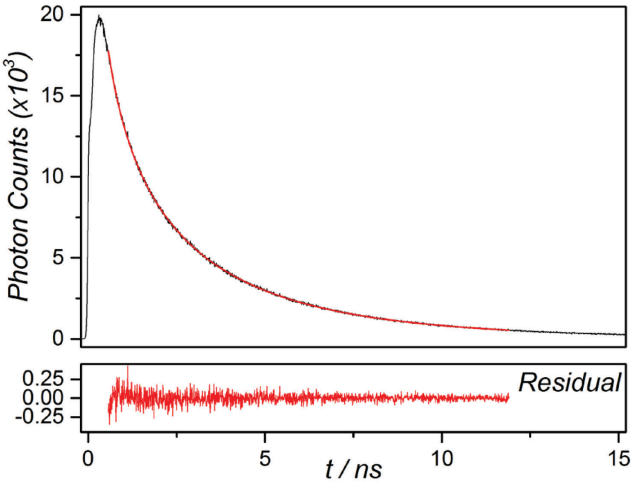


*Figure S.III.5. Time-correlated single photon counting decay curve (black) of PEGylated (4 mol%) DMPC liposomes **L23**, ([DMPC] = 0.2 mM) at 293 K with 0.5 mol% **2** and 0.9 mol% $\mathbf{3}^{2+}$ upon excitation with 440 nm (6 µW laser power, 0.6 pJ/pulse) and collecting emission at 474 nm. The red curve (top) represents a fit of the data according to a 3D FRET model (Equation S.III.12) with d = 3, τ = 6.2 ns, γ = 1.04, with the corresponding residual plot (bottom). The fit has an R^2 value of 0.9995.*

In the case of TA spectroscopy data, Equation S.III.12 was modified to Equation S.III.13:

$$\Delta OD(t,\lambda) = \Delta OD(\lambda)_0 \times e^{-\frac{t}{\tau_0} - 2\gamma\left(\frac{t}{\tau_0}\right)^{1/d}} \qquad \textit{Equation S.III.13}$$

where $\Delta OD(t,\lambda)$ is the observed time-dependent transient absorption spectrum and $\Delta OD(\lambda)_0$ is the transient absorption spectrum at t = 0. It was most convenient to use a kinetic trace at a particular wavelength to fit the data. Preliminary experiments with TA spectroscopy on **L2** and **L3** alone showed that 400 nm light excites both molecules, but that at 700 nm compound **2** has a major transient absorption peak while there is negligible signal of $\mathbf{3}^{2+}$ (see above). Therefore the kinetic trace at 700 nm was therefore selected for fitting with Equation S.III.13, *i.e.* λ = 700 nm. Similar to the fitting of TCSPC data, the TA data was indeed fitted using the model (Table S.III.4). Figure S.III.6 shows a fit of the three-dimensional model (d = 3) on lifetime decay data from TA at 293 K acquired from a liposome sample **L23** with 0.5 mol% **2** and 0.8 mol% $\mathbf{3}^{2+}$.

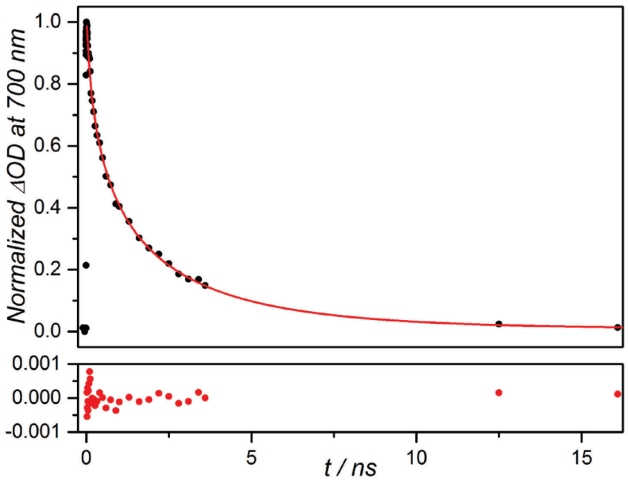


*Figure S.III.6. Transient absorption decay curve at 700 nm (black) of PEGylated (4 mol%) DMPC liposomes **L23** ([DMPC] = 20 mM) at 293 K with 0.5 mol% **2** and 0.8 mol% $\mathbf{3}^{2+}$ upon excitation with 400 nm (20-60 nJ/pulse, 1 KHz repetition rate). The red curve (top) represents a fit of the data according to a 3D FRET model (Equation S.III.12) with d = 3, τ = 6.0 ns, γ = 0.99, with the corresponding residual plot (bottom). The fit has a R^2 value of 0.997.*

The fitting parameters of the Förster three-dimensional decay model for both TCSPC and TA data, listed in Table S.III.2-Table S.III.4, show that for greater concentration of $\mathbf{3}^{2+}$, higher values of γ are obtained. In general, a three-dimensional model fitted the data better than a two-dimensional model, as the

3D model produced fits with X^2 values closer to 1. This agrees with the work of Holmes *et al.*[1, 10]

III.5.4. Calculating the experimental R_0 distance

The critical acceptor concentration C_0 (in M) is related to R_0 (in dm) by Equation S.III.14:

$$C_0 = \frac{3}{2\pi^{\frac{3}{2}} N_A R_0^3} \qquad \textit{Equation S.III.14}$$

so that a plot of γ *versus* [**3**] provided a straight line, of which the slope $1/C_0$ was used to evaluate R_0 (in dm), see Figure S.III.7. Again, [**3**] was substituted with $[\mathbf{3}]_{local}$ (see Equation S.III.9). In such conditions, R_0 was calculated to be 29 Å.

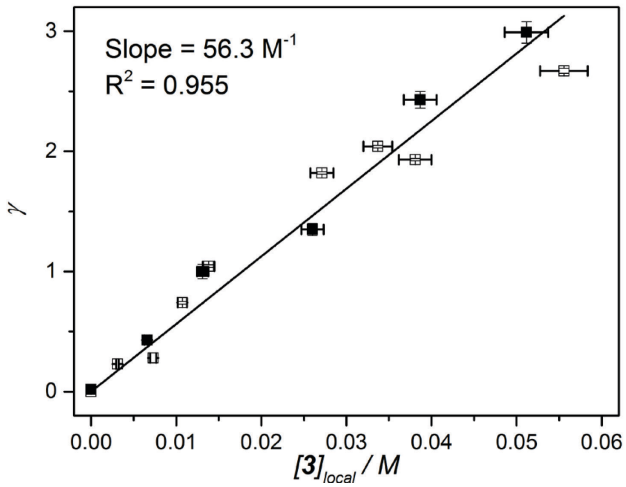


Figure S.III.7. Plot of γ at 293 K, as determined from transient absorption data (black filled squares) or from time-correlated single photon counting data (empty squares), as a function of the local concentration of $\mathbf{3}^{2+}$*, as defined by Equation S.III.9, in the lipid bilayer of PEGylated DMPC liposomes as determined by ICP-OES. Horizontal error bars represent 5% instrumental error from ICP-OES. Vertical error bars represent the fitting error of Equation S.III.12 on the data. The black line represents the best linear fit from the origin through the two combined data sets, and has a slope of 56.3* M^{-1} *with* $R^2 = 0.955$.

III.6. Photodissociation experiments using red light

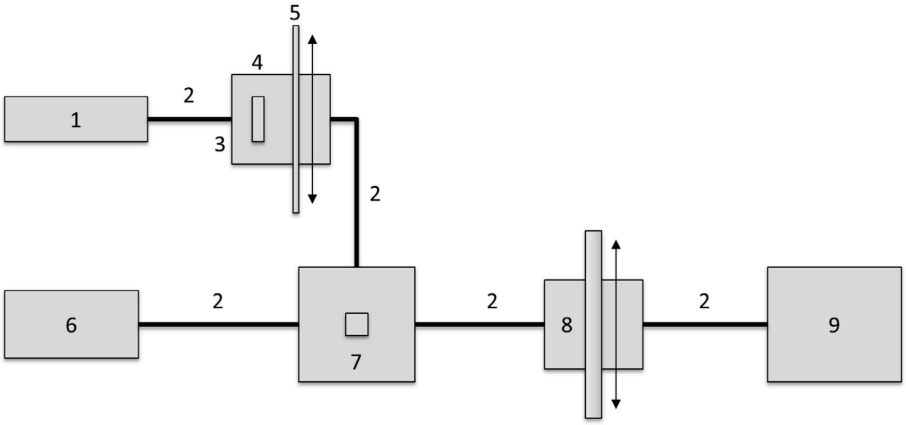


Figure S.III.8. Setup used for photosubstitution experiments using red light. Legend: (1) 630 nm laser source, (2) optical fibers, (3) filter holder, (4) 630 nm band pass filter, (5) variable neutral density filter that can be installed or removed, (6) halogen-deuterium light source for UV-Vis absorption spectroscopy, (7) temperature controlled cuvette holder, (8) variable filter holder, and (9) CCD spectrometer.

III.7. Definition and calculation of the total efficiency of TTA-UC, FRET and photodissociation

When TTA-UC and FRET are combined within the same membrane to realize the photochemical conversion of $\mathbf{3}^{2+}$ to $\mathbf{4}^{2+}$, the relevant photophysical and photochemical steps are

$$^1PS \xrightarrow{h\nu} {}^1PS^*$$

$$^1PS^* \xrightarrow{k_{ISC}} {}^3PS^*$$

$$^3PS^* + {}^1A \xrightarrow{k_{TTET}} {}^1PS + {}^3A^*$$

$$2\ {}^3A^* \xrightarrow{k_{TTA}} {}^1A + {}^1A^*$$

$$^1A^* + {}^1\mathbf{3}^{2+} \xrightarrow{k_{ET}} {}^1A + {}^1\mathbf{3}^{2+*}$$

$$^1\mathbf{3}^{2+*} \xrightarrow{k_{photosubstitution}} {}^1\mathbf{4}^{2+}$$

where for clarity purposes PS is the photosensitizer (**1**), and A is the annihilator (**2**), ISC means intersystem crossing, TTET means triplet-triplet energy transfer, TTA means triplet-triplet annihilation, and ET means non-radiative energy transfer. The rate of reaction is then defined by Equation S.III.15,

$$r = -\frac{dn_{\mathbf{3}^{2+}}}{dt} = \left|\frac{dn\,{}^{1}_{PS}}{dt}\right|_{created} \phi_{ISC}\phi_{TETT}\phi_{TTA}E_{ET}\phi_{Ru} \qquad \textit{Equation S.III.15}$$

where $\left|\frac{dn\,{}^{1}_{PS}}{dt}\right|_{created}$ is the rate of singlet state photosensitizer generated, φ_{ISC} is the QY of ISC of the photosensitizer, φ_{TETT} is the QY of TTET, φ_{TTA} is the QY of TTA, E_{ET} is the energy transfer efficiency as defined in Equation S.III.8, and φ_{Ru} is the quantum yield of photosubstitution in absence of **1** and **2**, measured under blue light irradiation. The rate of singlet state photosensitizer generated is further defined by Equation S.III.16:

$$\left|\frac{dn\,{}^{1}_{PS}}{dt}\right|_{created} = \Phi_{630}(1 - 10^{-A_{630}}) \qquad \textit{Equation S.III.16}$$

where Φ_{630} is the photon flux at 630 nm (einstein.s^{-1}) and A_{630} is the absorbance of the photosensitizer at 630 nm. In addition, similarly to Equation S.III.8, the efficiency of non-radiative energy transfer, E_{ET}, is given by Equation S.III.17:

$$E_{ET} = 1 - \frac{1}{1 + K_{SV} * [\mathbf{3}]_{local}} = \frac{K_{SV}[\mathbf{3}]_{local}}{1 + K_{SV}[\mathbf{3}]_{local}} \qquad \textit{Equation S.III.17}$$

where $[\mathbf{3}]_{local}$ is the local concentration of $\mathbf{3}^{2+}$ in the membrane, defined by Equation S.III.9 ($[\mathbf{3}]_{local} = \frac{n_{\mathbf{3}}}{n_{DMPC}V_M}$), and K_{SV} is the Stern-Volmer constant (L.mol^{-1}) for the quenching of ^{1}A* by $\mathbf{3}^{2+}$ in the lipid membrane. The quantum yield of TTA-UC is given by Equation S.III.18:

$$\phi_{ISC}\phi_{TETT}\phi_{TTA} = \phi_{TTA-UC} \qquad \textit{Equation S.III.18}$$

Thus Equation S.III.15 becomes Equation S.III.19:

$$r = -\frac{dn_{\mathbf{3}}}{dt} = \Phi_{630}(1 - 10^{-A_{630}})\phi_{TTA-UC}\frac{K_{SV}[\mathbf{3}]_{local}}{1 + K_{SV}[\mathbf{3}]_{local}}\phi_{Ru} \qquad \textit{Equation S.III.19}$$

Equation S.III.19 shows that the rate of the photosubstitution reaction depends on the local concentration of $\mathbf{3}^{2+}$ and a non-zero order reaction rate can be expected. Realizing that $K_{SV}[\mathbf{3}]_{\text{local}} << 1$, and that therefore E_{ET} can be approximated with $K_{SV}[\mathbf{3}]_{local} \equiv K_{SV}\frac{n_{\mathbf{3}}}{n_{DMPC}V_M}$, Equation S.III.19 simplifies to Equation S.III.20:

$$r = -\frac{dn_3}{dt} = \Phi_{630}(1 - 10^{-A_{630}})\phi_{TTA-UC}K_{SV}\frac{n_{\mathbf{3}}}{n_{DMPC}V_M}\phi_{Ru} \qquad \textit{Equation S.III.20}$$

Integrating Equation S.III.20 yields a first-order expression for $n_{\mathbf{3}}(t)$:

$$n_{\mathbf{3}}(t) = n_{\mathbf{3}}(0) * e^{-kt} \qquad \textit{Equation S.III.21}$$

where k is given by Equation S.III.22:

$$k = \frac{\Phi_{630}}{n_{DMPC}V_M}(1 - 10^{-A_{630}})\phi_{TTA-UC}K_{SV}\phi_{Ru} \qquad \textit{Equation S.III.22}$$

The total efficiency of TTA-UC, FRET, and photodissociation of $\mathbf{3}^{2+}$ in liposomes **L123** is defined by Equation S.III.23:

$$E_{total} = \phi_{TTA-UC}E_{ET}\phi_{Ru} \approx \phi_{TTA-UC}K_{SV}\frac{n_{\mathbf{3}}}{n_{DMPC}V_M}\phi_{Ru} \qquad \textit{Equation S.III.23}$$

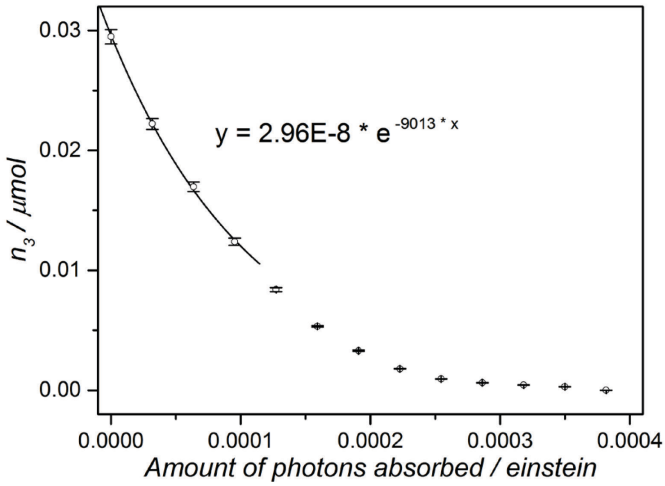


*Figure S.III.9. Plot of n_3 as a function of the amount of photons absorbed during the photodissociation experiment with red light of **L123**. The black line represents a single exponential fit for the first 45 min of irradiation.*

For t = 0 – 45 min, *i.e.* when E_{ET} is more or less constant, E_{total} can be experimentally determined from a plot of the amount of mol of $\mathbf{3}^{2+}$ as a function of the amount of absorbed photons, *i.e.* $\Phi_{630} * (1 - 10^{-A_{630}}) * t$, see Figure S.III.9. Φ_{630} was estimated from measuring the optical power (120 mW at 630 nm, *i.e.* 0.632 µeinstein.s^{-1}) and A_{630} was 0.025. Note that at t = 0, mostly **1** absorbs at 630 nm. Some bleaching of **1** was observed during the reaction (Figure 4.3b), but it was neglected in this calculation. Therefore, the amount of absorbed photons per unit time was considered to be constant. E_{total} at t = 0 can be evaluated from the slope at t = 0 of the single exponential fit curve of the evolution of n_3 *versus* the amount of red photons absorbed since t = 0 (see Figure S.III.9). From this, a value of 0.027% was determined.

The amount of mol $\mathbf{3}^{2+}$ was determined from the UV-VIS absorbance data at 490 nm by accounting for the contributions of both $\mathbf{3}^{2+}$ and $\mathbf{4}^{2+}$ to the absorption at this wavelength, as explained here. The total absorbance at 490 nm is given by Equation S.III.24:

$$A^{490} = \varepsilon_{\mathbf{3}}^{490} \times l \times [\mathbf{3}] + \varepsilon_{\mathbf{4}}^{490} \times l \times [\mathbf{4}] \qquad \textit{Equation S.III.24}$$

where $\varepsilon_{\mathbf{3}}^{490}$ is the molar absorption coefficient of $\mathbf{3}^{2+}$ at 490 nm (3760 M^{-1}.cm^{-1} in $CHCl_3$), [**3**] is the bulk concentration of $\mathbf{3}^{2+}$, $\varepsilon_{\mathbf{4}}^{490}$ is the molar absorption

coefficient of $\mathbf{4}^{2+}$ at 490 nm (8690 $M^{-1}.cm^{-1}$ in H_2O), [**4**] is the bulk concentration of $\mathbf{4}^{2+}$, and l is the cuvette path length (*i.e.* 1 cm). At $t = \infty$, the photoreaction is complete and no more $\mathbf{3}^{2+}$ is present, which means that

$$A_{\infty}^{490} = \varepsilon_{\mathbf{4}}^{490} \times l \times [\mathbf{3}]_0 \qquad \textit{Equation S.III.25}$$

By replacing [**4**] with $[\mathbf{3}]_0 - [\mathbf{3}]$ in Equation S.III.24, [**3**] can be expressed as a function of A^{490} in Equation S.III.26:

$$[\mathbf{3}] = \frac{A^{490} - A_{\infty}^{490}}{\varepsilon_{\mathbf{3}}^{490} \times l - \varepsilon_{\mathbf{4}}^{490} \times l} \qquad \textit{Equation S.III.26}$$

Finally, the amount of mol $\mathbf{3}^{2+}$ is obtained by multiplying with the volume in the cuvette (*V*, *i.e.* 1.5 ml), see Equation S.III.27:

$$n_{\mathbf{3}} = V * \frac{A^{490} - A_{\infty}^{490}}{\varepsilon_{\mathbf{3}}^{490} - \varepsilon_{\mathbf{4}}^{490}} \qquad \textit{Equation S.III.27}$$

At $t = 0$, the value for n_3 ($2.95 \times 10^{-8} \pm 0.06 \times 10^{-8}$ mol) was very comparable with the value for n_3 determined by ICP-OES ($2.82 \times 10^{-8} \pm 0.01 \times 10^{-8}$) , which confirms the validity of this approach.

III.8. Photodissociation experiments with lower red-light intensities

Irradiation experiments on liposomes **L123** were repeated with three different red light intensities of 30, 60, and 120 mW (0.24, 0.48, and 0.95 $W.cm^{-2}$, respectively). The course of the reaction was monitored by UV-Vis absorption spectroscopy following the absorbance of the aqua photoproduct at 490 nm (Figure S.III.10). As expected, a decrease in reaction rate was observed for lower irradiation intensities (Figure S.III.10d). To determine the total efficiency of the system (E_{total}, see Equation S.III.23), the amount of ruthenium (n_3) was plotted *versus* the amount Q of photons absorbed since $t = 0$ (Figure S.III.11). E_{total} was calculated from the exponential fit of the data by multiplying the exponent with the amplitude, yielding values of 0.026% for 0.24 $W.cm^{-2}$, 0.024% for 0.48 $W.cm^{-2}$, and 0.019% for 0.95 $W.cm^{-2}$. The

somewhat lower quantum yield for the experiment using 0.95 W.cm^{-2} irradiation is attributed to some bleaching of the photosensitizer (**1**) in this particular experiment (compare A_{630} at t = 180 between the three individual experiments in Figure S.III.10). The real amount of photons absorbed by **1** is therefore lower (*i.e.* the real quantum yield is higher), but the data is not corrected for this effect. Overall, all three efficiencies values E_{total} were found very similar to that given in the main text (0.027% for 0.95 W.cm^{-2} red light irradiation), so it can be concluded that the quantum efficiency of red light-induced photosubstitution in **L123** is unaffected by light intensity and this range of intensities.

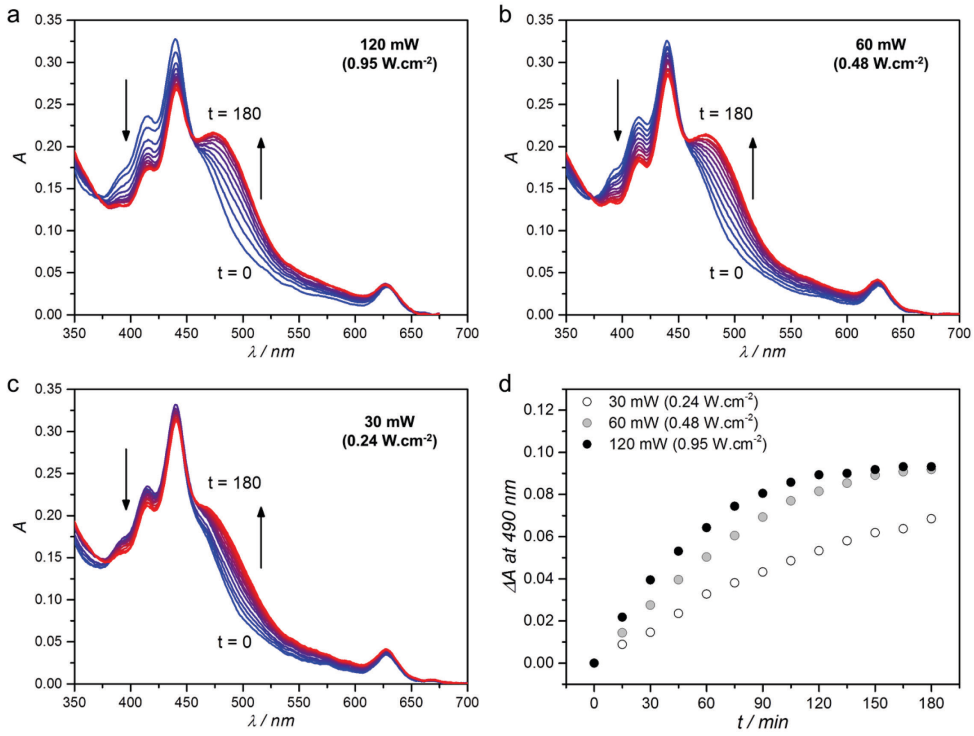


*Figure S.III.10. Absorption spectra of liposomes **L123** during red light irradiation (630 nm) with (a) 30 mW (0.24 W.cm^{-2}), (b) 60 mW (0.48 W.cm^{-2}), and (c) 120 mW (0.95 W.cm^{-2}). Blue line: spectrum at t = 0; red line: spectrum at t = 180 minutes; other spectra measured every 15 minutes. d) Difference in absorbance at 490 nm, after baseline correction, during red-light irradiation of **L123** with 30 mW (white), 60 mW (grey), or 120 mW (black). T = 310 K, sample volume 1.5 ml, 8% of sample volume simultaneously irradiated. A single **L123** liposome stock dispersion was used in these experiments and diluted with PBS buffer prior to measurement so that every time [**1**] = 0.25 μM, and [**2**] = 2.5 μM.*

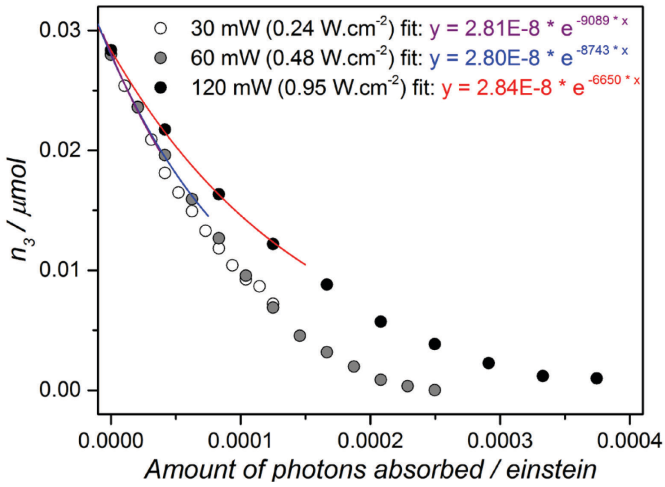


Figure S.III.11. Evolution of the number of mol of $\mathbf{3}^{2+}$ *(*n_3*) as a function of the amount of red photons absorbed since t = 0 for liposome sample* ***L123*** *irradiated with 30 mW (0.24 W.cm*$^{-2}$ *white circles, purple fit curve), 60 mW (0.48 W.cm*$^{-2}$*, grey circles, blue fit curve), or 120 mW (0.95 W.cm*$^{-2}$*, black circles, red fit curve). The fit lines represent single exponential fits for the first 45 min of irradiation for each dataset. The lower slope for the 120 mW experiment is attributed to more bleaching of the photosensitizer during irradiation.*

III.9. References

[1] A. S. Holmes, D. J. S. Birch, T. Salthammer, *J. Fluoresc.* **1993**, *3*, 77-84.
[2] S. L. Joris J. Snellenburg, Ralf Seger, Katharine M. Mullen, Ivo H. M. van Stokkum, *J. Stat. Softw.* **2012**, *49*, 1-22.
[3] Y. H. Meyer, P. Plaza, *Chem. Phys.* **1995**, *200*, 235-243.
[4] S. Bonnet, B. Limburg, J. D. Meeldijk, R. J. M. Klein Gebbink, J. A. Killian, *J. Am. Chem. Soc.* **2010**, *133*, 252-261.
[5] N. H. Damrauer, G. Cerullo, A. Yeh, T. R. Boussie, C. V. Shank, J. K. McCusker, *Science* **1997**, *275*, 54-57.
[6] J. R. Lakowicz, *Principles of Fluorescence Spectroscopy*, 3rd ed., Springer Science+Business Media, LLC, New York, NY, USA, **2006**.
[7] J. T. Buboltz, C. Bwalya, S. Reyes, D. Kamburov, *J. Chem. Phys.* **2007**, *127*, 215101.
[8] D. Marsh, *Handbook of Lipid Bilayers*, 2nd ed., Taylor & Francis Group, LLC, Boca Raton, FL, USA, **2013**.
[9] I. B. Berlman, *Handbook of fluorescence spectra of aromatic molecules*, 2nd ed., Academic Press, New York, NY, USA, **1971**.
[10] A. S. Holmes, K. Suhling, D. J. S. Birch, *Biophys. Chem.* **1993**, *48*, 193-204.

APPENDIX IV: SUPPORTING INFORMATION FOR CHAPTER 5

IV.1. Cryo transmission electron microscopy

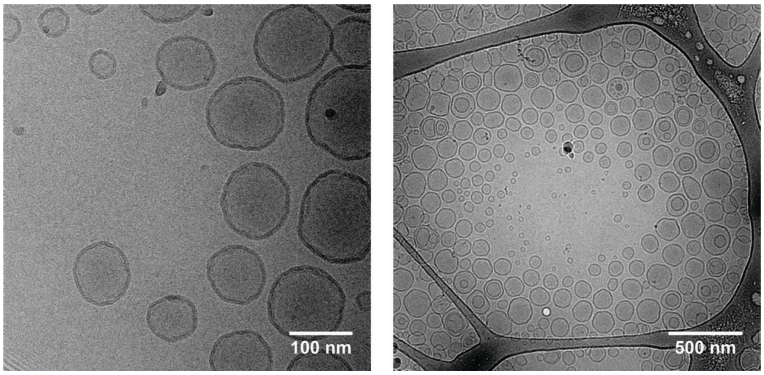


*Figure S.IV.1. Cryo transmission electron micrographs of DMPC **LUV12**.*

IV.2. Emission spectroscopy on LUVs

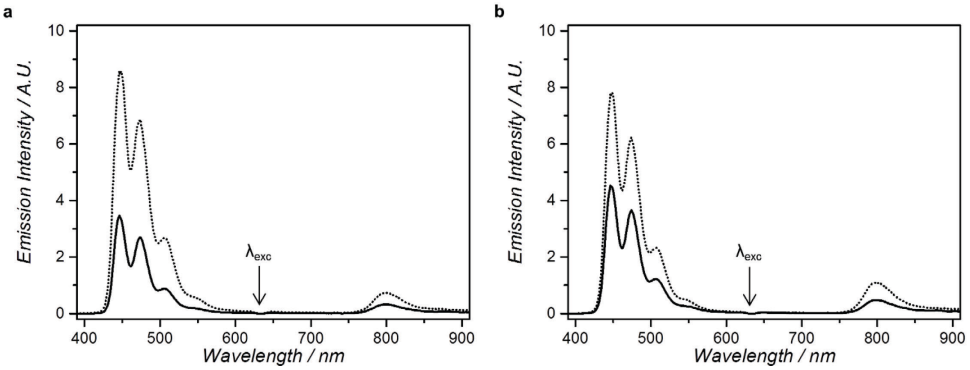


*Figure S.IV.2. Emission spectra of DOPC (a) and DMPC (b) **LUV12** samples ([lipid] = 1 mM, [DSPE-PEG-2000] = 0.04 mM, [**2**] = 5 μM, [**1**] = 0.25 μM) under 630 nm excitation at 298 K. The samples were either deoxygenated by bubbling argon for 30 min prior to measurement (solid curves) or by addition of sodium sulfite at a concentration of 0.3 M to the buffer (dotted curves). Irradiation conditions: 3.0 mL sample volume in a macro fluorescence cuvette, with 30 mW 630 nm irradiation power (4 mm beam diameter, intensity 0.24 W.cm^{-2}). Bubbling of argon through the sample inevitably results in the formation of small bubbles on the walls of the measurement cuvette, resulting in scattering of light in both the excitation and the detection pathway. These bubbles are absent in the case of deoxygenation using the sodium sulfite oxygen scavenger, which explains why the observed intensities are higher for samples deoxygenated with sulfite.*

IV.3. Emission spectroscopy on GUVs

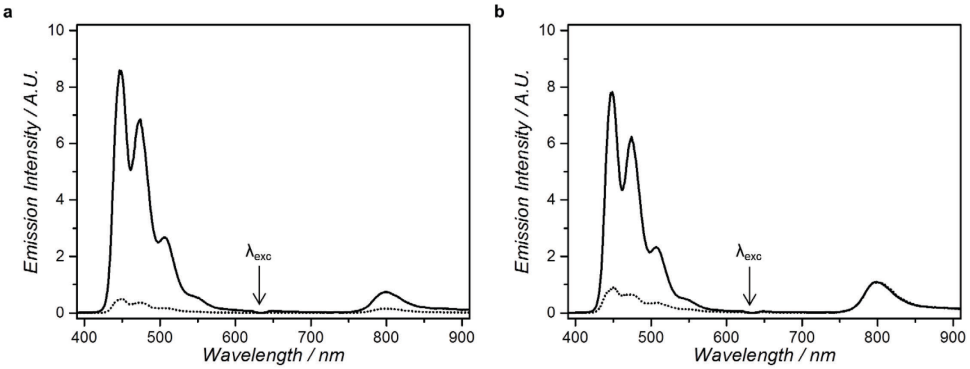


Figure S.IV.3. Emission spectra of DOPC (a) and DMPC (b) ***LUV12*** *(solid curves) and* ***GUV12*** *(dotted curves) with 30 mW 630 nm excitation (0.24 W.cm² intensity) at 298 K. In the case of LUVs, [DMPC] = 1 mM, [DSPE-PEG-2000] = 0.04 mM, [**2**] = 5 µM, [**1**] = 0.25 µM, whereas in the case of GUVs, the lipid concentration was not known, but the components in the membrane were introduced in the same molar ratio as for the LUV samples. In all cases, the buffer was deoxygenated by addition of sodium sulfite (0.3 M) and the spectra were measured under air.*

IV.4. Power dependency measurements

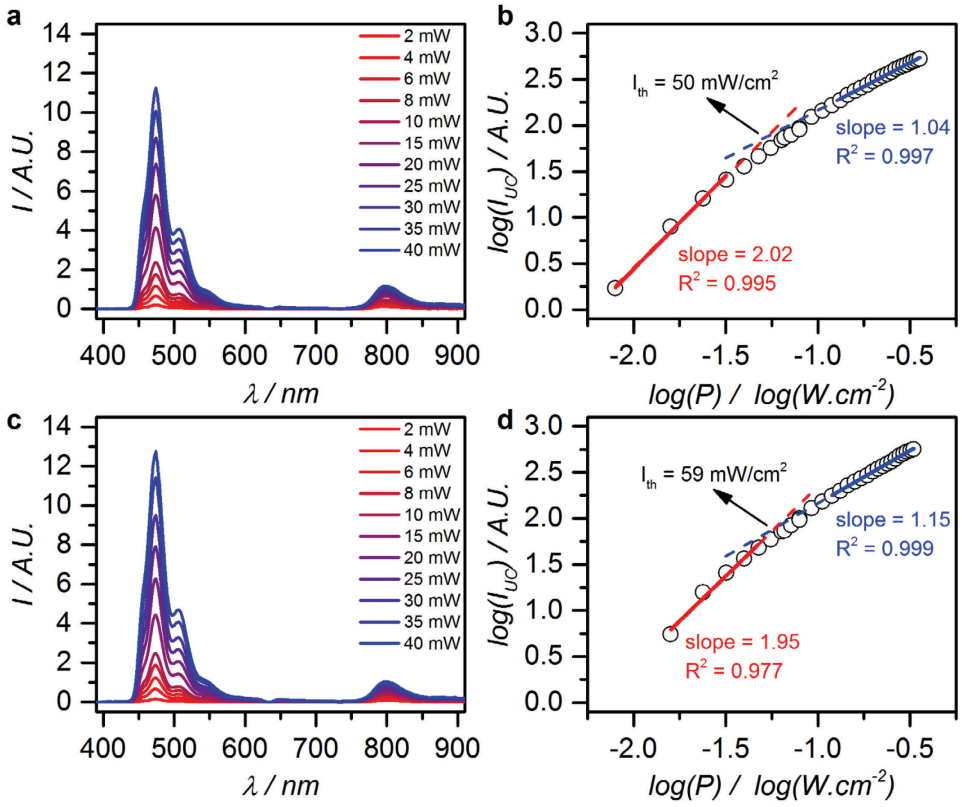


*Figure S.IV.4. Luminescence emission spectra of DMPC **LUV-12** (a) and DOPC **LUV-12** (c) at various excitation intensities. Double logarithmic plot of the upconversion luminescence intensity (I_{UC}) of DMPC **LUV-12** (b) and DOPC **LUV-12** (d), integrated from 420 to 575 nm, as a function of the excitation intensity P (in W.cm^{-2}). The low power regime was fitted with straight lines with slopes 2.02 (R^2 = 0.995) and 1.95 (R^2 = 0.977) for DMPC and DOPC **LUV-12**, respectively (red solid lines), and the high power regime was fitted with straight lines with slopes 1.04 (R^2 = 0.997) and 1.15 for DMPC and DOPC **LUV-12**, respectively (blue solid lines). From the intersection of the extrapolated fits (red and blue dashed lines), the intensity threshold (I_{th}) was found to be 50 mW.cm^{-2} for DMPC **LUV-12** and 59 mW.cm^{-2} for DOPC **LUV-12**. Irradiation conditions: [lipid] = 1.0 mM, T = 298 K, laser beam diameter 4 mM.*

IV.5. Microscopy imaging

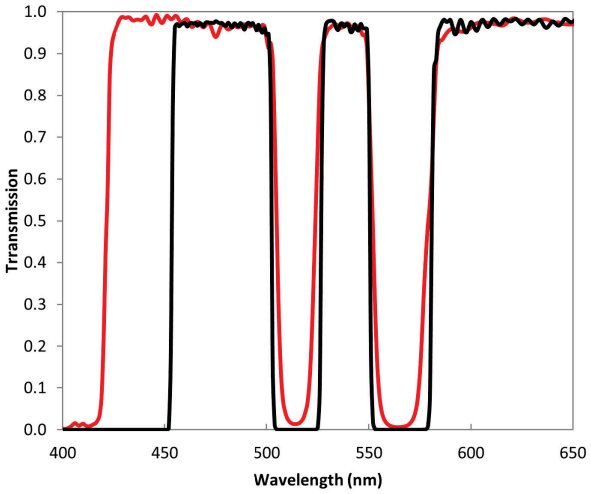


Figure S.IV.5. Transmission curves of the filter and dichroic beam splitter that were used for emission microscopy with violet light (405 nm), consisting of a Chroma ZT405/514/561rpc dichroic beam splitter (red) and a Chroma ZET442/514/568m emission filter (black).

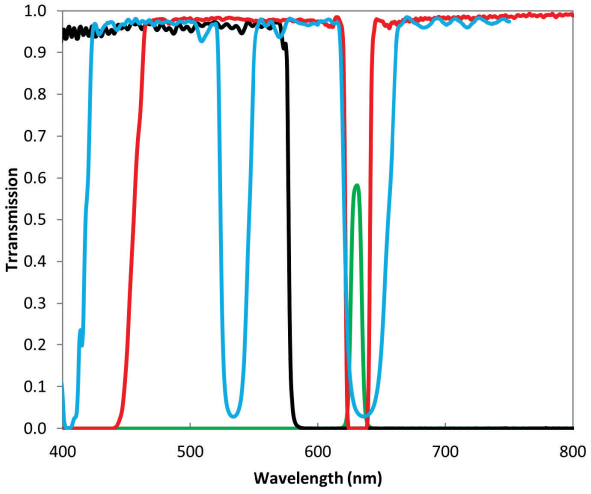


Figure S.IV.6. Transmission curves of the filters and dichroic beam splitter that were used for emission microscopy with red light (630 nm), consisting of a Thorlabs NF633-25 notch filter (red) and an Edmund Optics 575 nm OD4 short pass filter (black), a Thorlabs FB630-10 band pass filter (green), and a Chroma ZT405/532/635rpc dichroic mirror (blue).

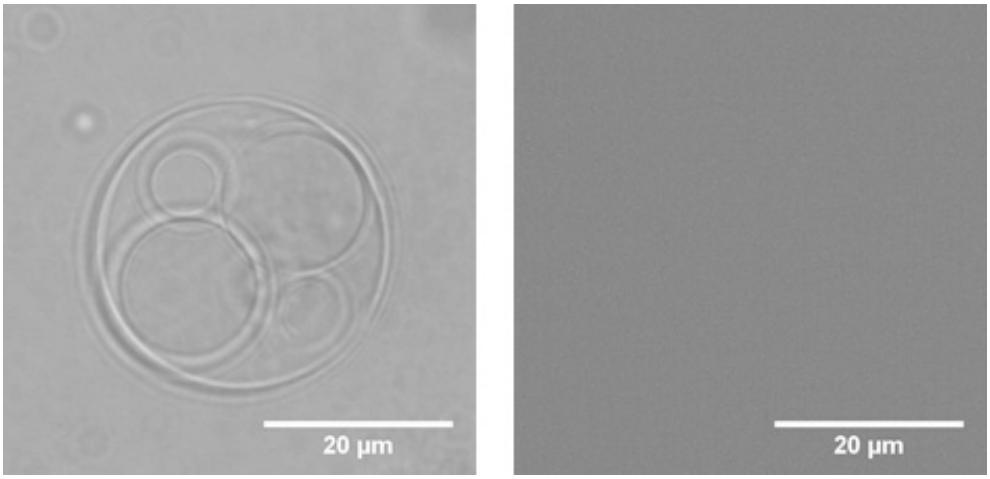


*Figure S.IV.7. Bright field (left) and upconversion emission (right) photographs of DOPC **GUV2**, i.e. GUVs similar to **GUV12** but deprived of the photosensitizer 1, in buffer without sodium sulfite and under air atmosphere.*

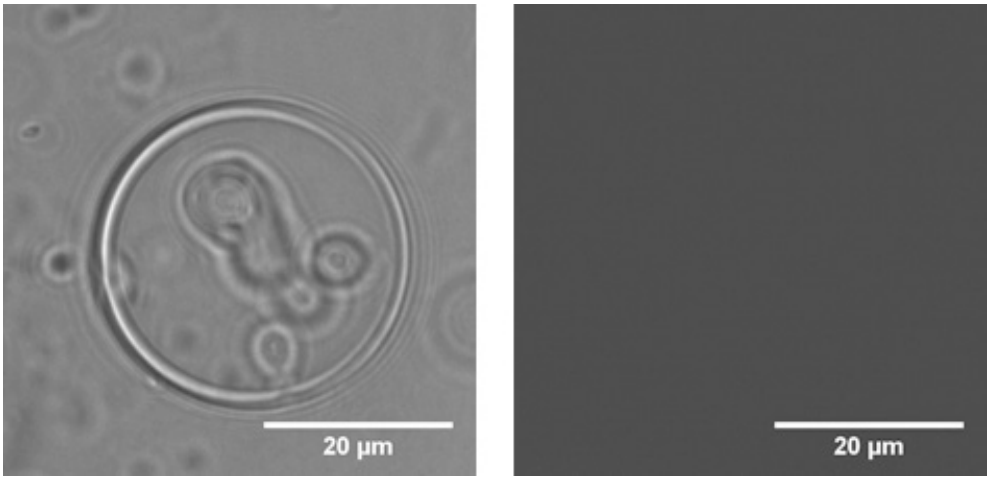


*Figure S.IV.8. Bright field (left) and upconversion emission (right) photographs of DOPC **GUV12** in air atmosphere in buffer without sodium sulfite.*

APPENDIX V: SUPPORTING INFORMATION FOR CHAPTER 6

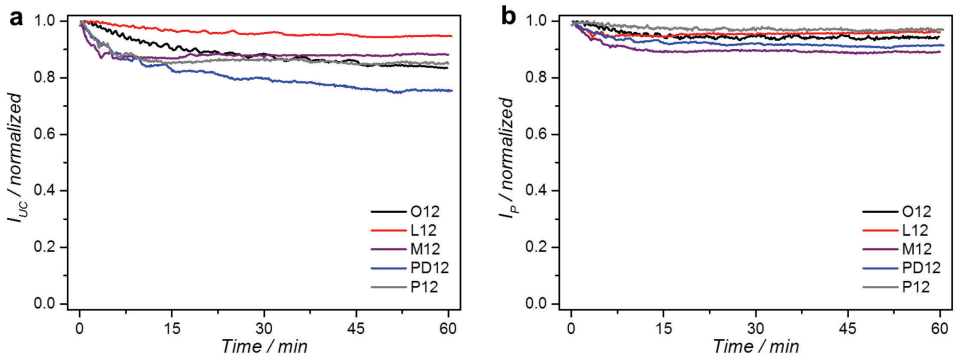


*Figure S.V.1. Time dependence of I_{UC} and I_P at 20 °C of samples **O12**, **L12**, **M12**, **PD12**, and **P12**. All samples show an initial drop in phosphorescence, followed by stabilization. Considering that trace amounts of oxygen are still present at t = 0, we attribute this to the generation of singlet oxygen by the photosensitizer upon light excitation and reaction of singlet oxygen with the photosensitizer and/or annihilator.*

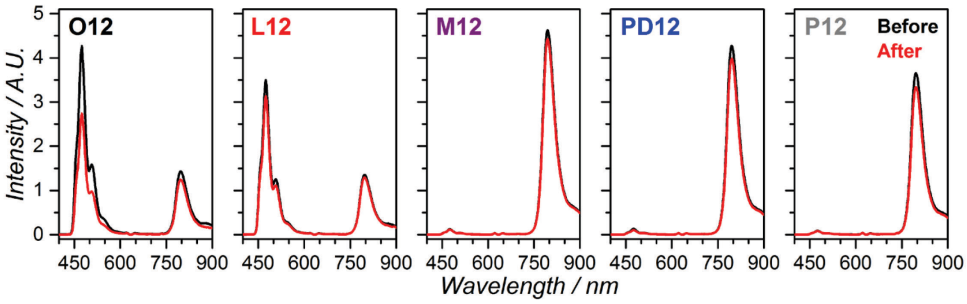


*Figure S.V.2. Luminescence spectra of samples **O12**, **L12**, **M12**, **PD12**, and **P12** at 5°C before (black) and after (red) heating from 5 °C to 50 °C and continuous red light irradiation. Spectra taken with 10 mW (80 mW.cm^{-2}) 630 nm excitation. Only **O12** shows significant bleach.*

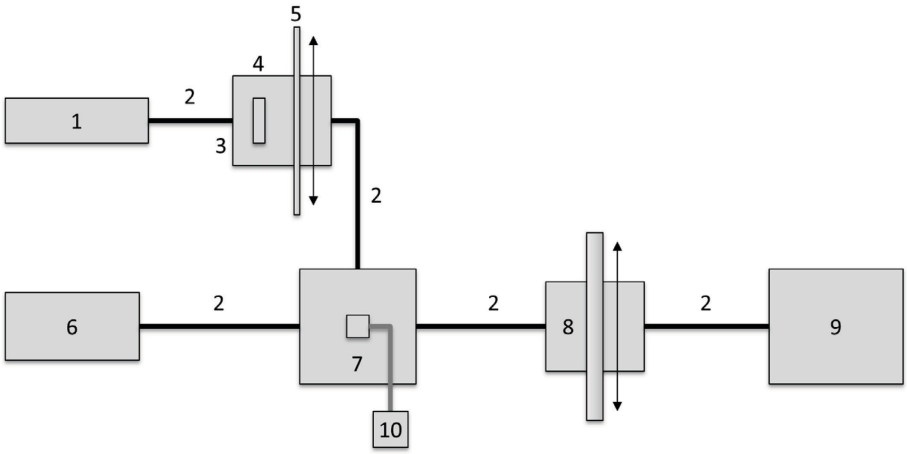


Figure S.V.3. Setup used for emission spectroscopy. Legend: (1) 630 nm laser source, (2) optical fibers, (3) filter holder, (4) 630 nm band pass filter, (5) variable neutral density filter that can be installed or removed, (6) halogen-deuterium light source for UV-Vis absorption spectroscopy, (7) temperature controlled cuvette holder, (8) variable filter holder, (9) CCD spectrometer, and (10) temperature probe submerged in the sample.

APPENDIX VI: SUPPORTING INFORMATION FOR CHAPTER 7

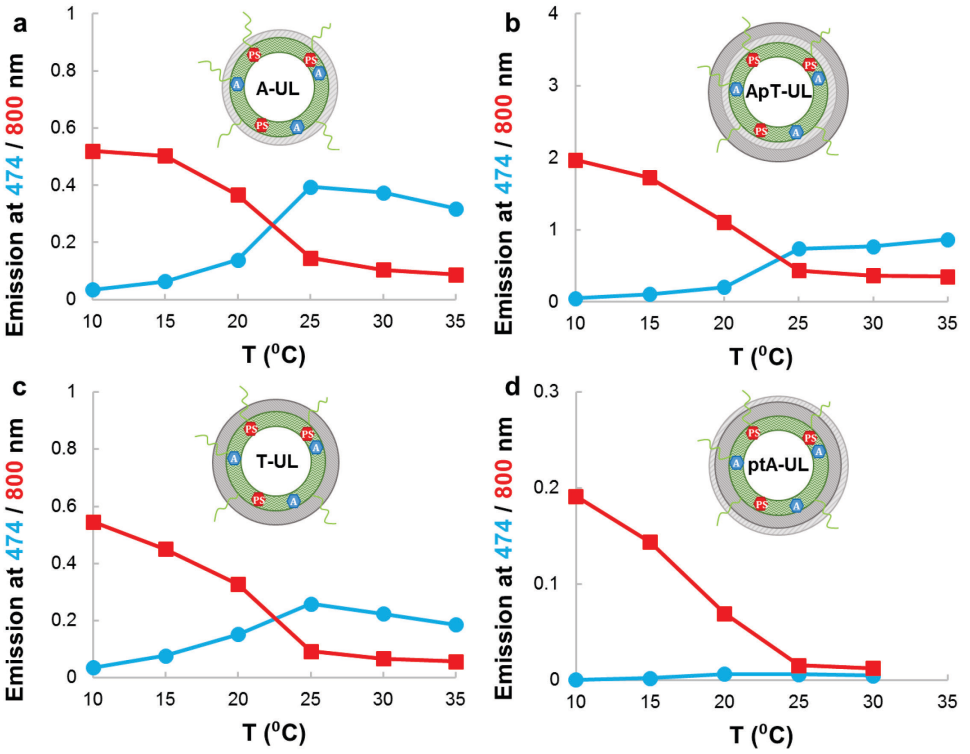


*Figure S.VI.1. Temperature dependencies of upconversion (at 475 nm, blue circles) and phosphorescence (at 800 nm, red squares) for **A-UL** (a), **ApT-UL** (b), **T-UL** (c), and **pTA-UL** (d) in 50 mM Na_2SO_3 PBS with 30 mW 630 nm (240 mW.cm^{-2}).*

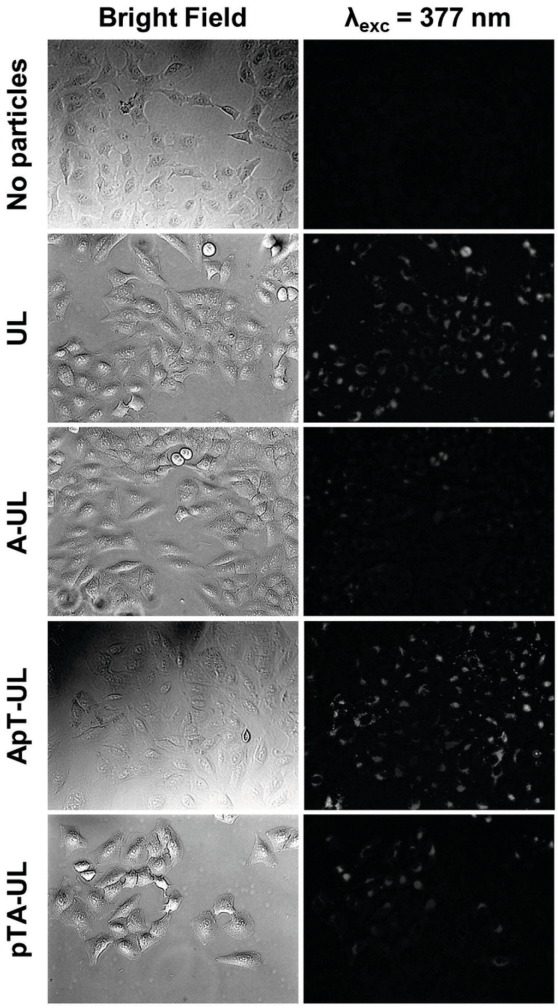


*Figure S.VI.2. Microscopy imaging in bright field mode (left column) and with 377 nm excitation (right column) of A549 cells treated with either **UL**, **A-UL**, **ApT-UL**, **pTA-UL**, or no particles as control.*

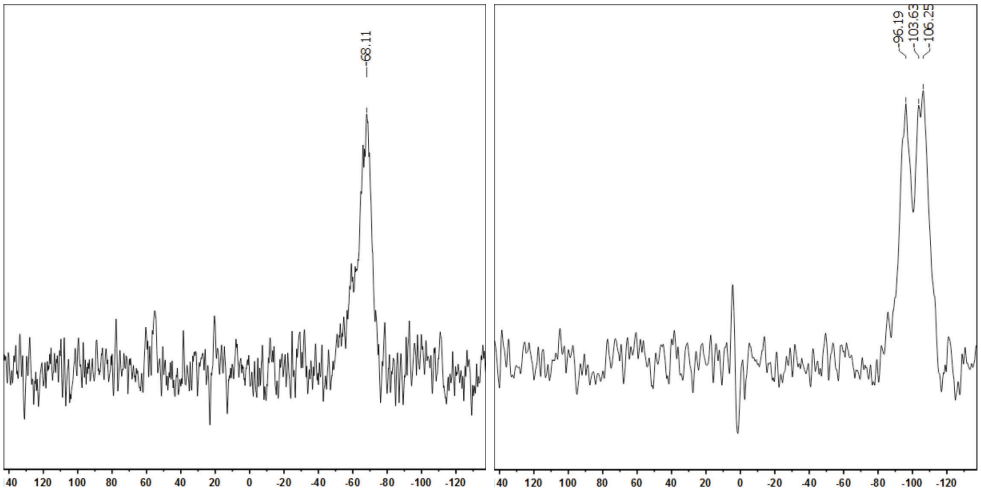


*Figure S.VI.3. ^{29}Si-NMR spectra of samples **A-UL-D** (left) and **ApT-UL-D** (right).*

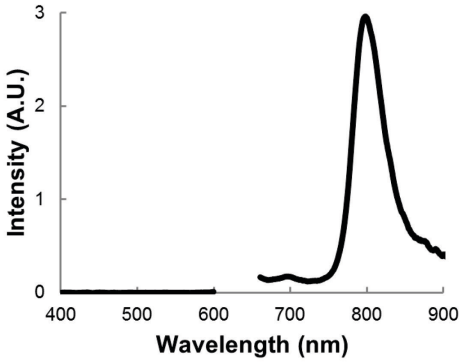


*Figure S.VI.4. Emission spectrum of freeze-dried upconverting liposomes (**UL-F**) under 30 mW 630 nm excitation (0.66 W.cm^{-2}) at 20 °C.*

APPENDIX VII: SUPPORTING INFORMATION FOR CHAPTER 8

VII.1. Hopping of perylene (compound 2) *versus* 2,5,8,11-tetra(*tert*-butyl)perylene (compound 3)

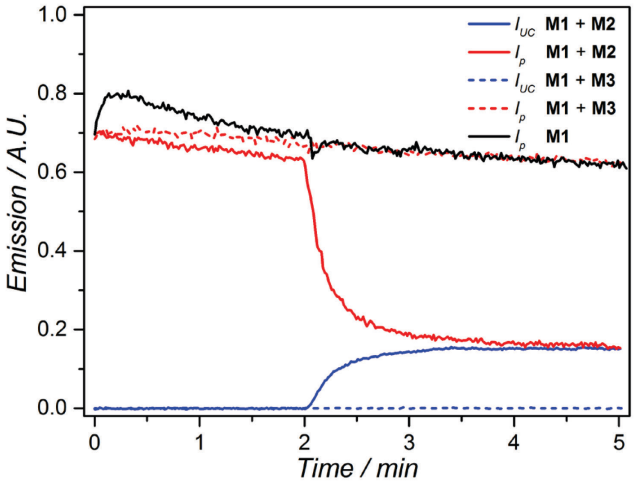


*Figure S.VII.1. Hopping of compound **2** versus compound **3** by monitoring TTA-UC upon mixing **M1** with either **M2** or **M3**. A diluted sample of **M1** liposomes (0.25 mM DMPC) in 0.1 M Na_2SO_3 in PBS was placed in a stirred macro cuvette at 25 °C and the emission spectrum was acquired for 2 min with 10 mW 630 nm (80 mW.cm^{-2}). At t = 2 min, 1 equivalent of either **M2**, **M3**, or only PBS (all containing 0.1 M Na_2SO_3) was added and spectra were continuously acquired. The upconversion intensity (I_{UC}) at 474 nm (**2**) or 486 nm (**3**), and the phosphorescence intensity (I_P) at 800 nm (**1**) are plotted versus time.*

It is known in the literature that perylene (compound **2**) partitions with the aqueous phase when dissolved in the lipid bilayer of liposomes.[1] To prevent perylene from escaping the vesicles, 2,5,8,11-tetra(*tert*-butyl)perylene (compound **3**) was synthesized (see Chapter 9, section 9.4.2). In order to investigate whether tert-butylation made the compound more membrane-bound, a "hopping" experiment was conducted as follows. Three different PEGylated DMPC liposome samples were prepared in 0.1 M Na_2SO_3 in PBS: one containing only photosensitizer **1** (**M1**), one containing only perylene **2** (**M2**), and one containing only tert-butylated perylene **3** (**M3**). Then, **M1** was placed in a stirred cuvette at 25 °C and the emission spectrum was continuously acquired under 10 mW 630 nm irradiation (80 mW.cm^{-2}). After

2 min, **M2** was added and the emission spectrum was acquired for 3 more min. The same experiment was also performed with using **M3** instead of **M2**. As a control, the emission of **M1** was monitored for 5 min without further liposome addition. In Figure S.VII.1, the upconversion intensity (I_{UC}) and phosphorescence intensity of **1** (I_p) are plotted versus time. Upon addition of **M2** to **M1**, upconversion was instantaneously observed and stabilized 1 min after mixing, while the phosphorescence was quenched and also stabilized after 1 min after mixing. Note that TTA-UC requires molecular contact, and that the liposomes do not fuse or come in close proximity of each other due their PEGylated surface. Thus, under the assumption that **1** does not hop, these results indicate that compound **2** had hopped from **M2** to **M1** within this time, which is consistent with the observations of Almgren.[1] For the mixture of **M1** and **M3**, no phosphorescence quenching was observed and no upconversion was observed throughout the experiment. From this, it can be concluded that neither compound **3** nor compound **1** escapes DMPC membranes. Overall, these results demonstrate that four-fold *t*-butylation of perylene indeed prevents liposomal escape.

VII.2. Fluorescence spectrum of LysoTracker Red

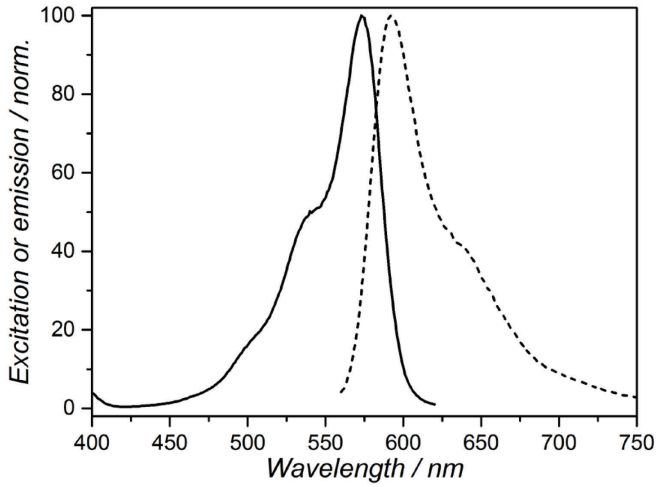


Figure S.VII.2. Normalized excitation (solid) and emission spectrum (dashed) of LysoTracker Red DND-99. Data acquired from manufacturer ThermoFisher Scientific.

VII.3. Uptake of M1, M3, and M1-3 liposomes in cells

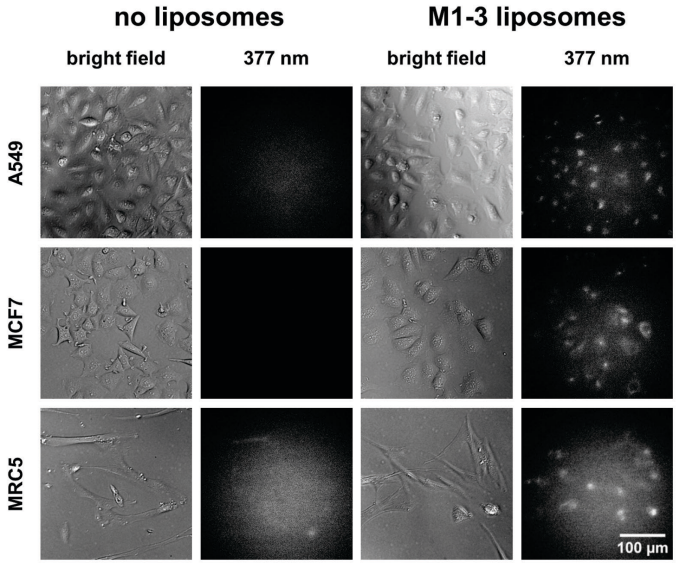


*Figure S.VII.3. Bright field and fluorescence micrographs (λ_{exc} = 377 nm) at 20x magnification of A549 (top row), MCF7 (middle row), and MRC5 cells (bottom row) that were incubated with no liposomes (left side) and **M1-3** liposomes (right side) for 24h.*

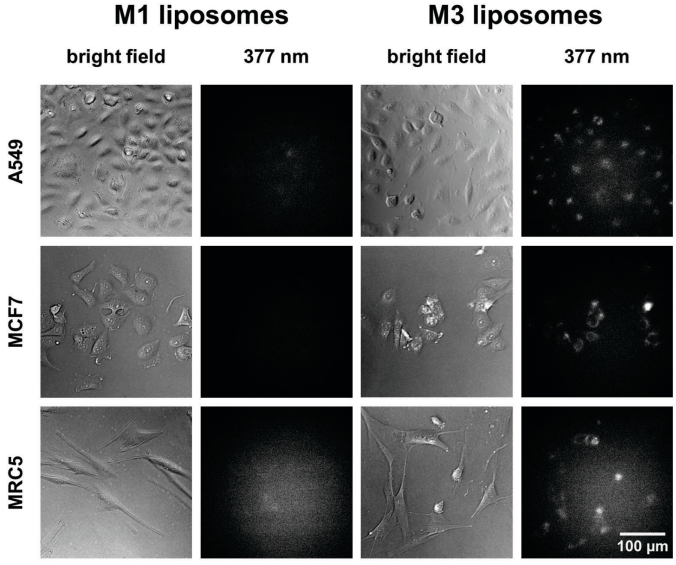


*Figure S.VII.4. Bright field and fluorescence micrographs (λ_{exc} = 377 nm) at 20x magnification of A549 (top row), MCF7 (middle row), and MRC5 cells (bottom row) that were incubated with **M1** liposomes (left side) and **M3** liposomes (right side) for 24h. Note that **M1** liposomes are not fluorescent and only autofluorescence is observed.*

VII.4. Overlap between absorption of Ru-complexes 5^{2+}, 6^{2+}, 7^{2+} and 8^{2+} and emission of compound 3

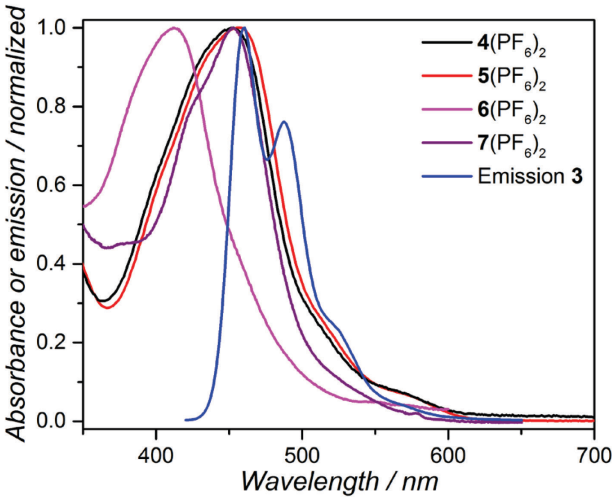


*Figure S.VII.5. Overlap between normalized absorption spectra of Ru-complexes **5**$^{2+}$, **6**$^{2+}$, **7**$^{2+}$ and **8**$^{2+}$ and the normalized emission spectrum of compound **3**.*

VII.5. Photosubstitution of Ru-complexes 5^{2+}, 6^{2+}, and 7^{2+} with blue light

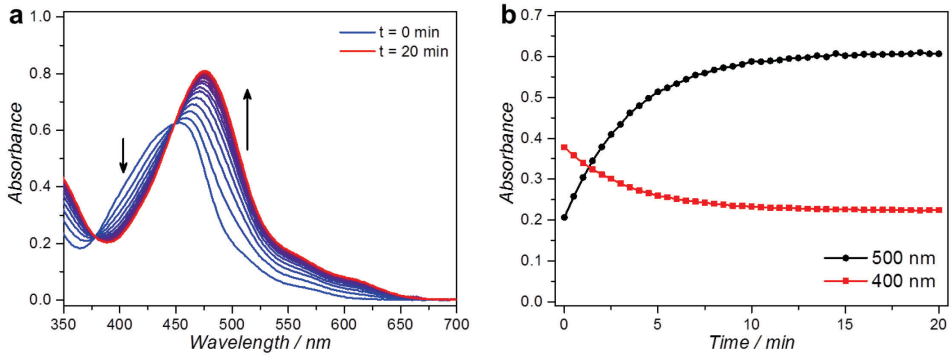


*Figure S.VII.6. Time-dependent UV-vis absorption spectroscopy of complex **5**$^{2+}$ (0.1 mM) during blue light irradiation (450 nm, photon flux 0.17 µEinstein.s^{-1}) in water at 25 °C. a) Absorption spectra, recorded every 1 min (blue to red evolution). b) Evolution of the absorbance at 400 nm (red squares) and 500 nm (black circles). The water was deoxygenated for 10 min by bubbling with argon and the solution was kept under an argon atmosphere during spectroscopy. The quantum yield of photosubstitution of converting **5**$^{2+}$ to **8**$^{2+}$ was calculated to be 0.70% according to a previously published method.[2]*

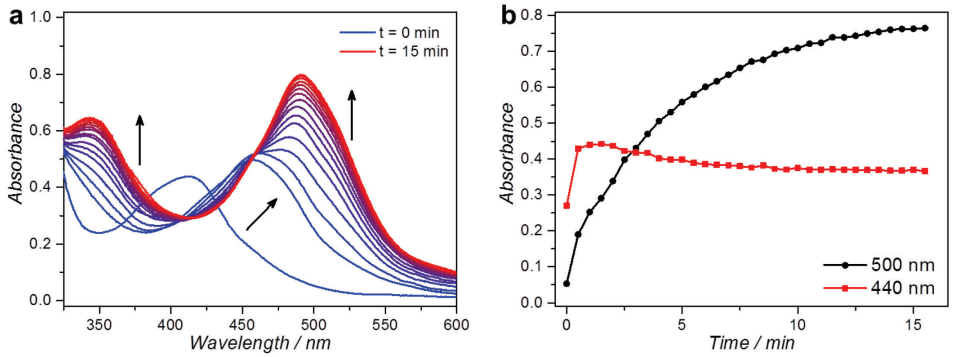


Figure S.VII.7. Time-dependent UV-vis absorption spectroscopy of complex $\mathbf{6}^{2+}$ *(0.07 mM) during blue light irradiation (450 nm, photon flux 0.17 µEinstein.s*$^{-1}$*) in water at 25 °C. a) Absorption spectra, recorded every 1 min (blue to red evolution). b) Evolution of the absorbance at 440 nm (red squares) and 500 nm (black circles). The water was deoxygenated for 10 min by bubbling with argon and the solution was kept under an argon atmosphere during spectroscopy. The spectral evolution upon reaction of* $\mathbf{6}^{2+}$ *to* $\mathbf{9}^{2+}$ *shows that the photoreaction proceeds via two distinct steps: it is proposed that the first step is fast and involves the release of one of the thioether-ruthenium bonds (see how the spectrum changes in the first minute), and the second step is slower and involves the release of the other thioether-ruthenium bond.*

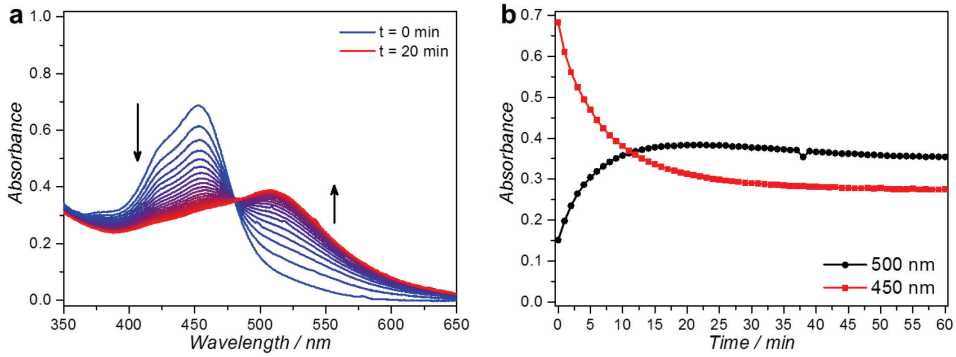


Figure S.VII.8. Time-dependent UV-vis absorption spectroscopy of complex $\mathbf{7}^{2+}$ *(0.070 mM) during blue light irradiation (450 nm, photon flux 0.17 µEinstein.s*$^{-1}$*) in 9:1 v/v acetone:*H_2O *at 25 °C. a) Absorption spectra, recorded every 1 min (blue to red evolution). b) Evolution of the absorbance at 450 nm (red squares) and 500 nm (black circles). The water was deoxygenated for 10 min by bubbling with argon and the solution was kept under an argon atmosphere during spectroscopy.*

VII.6. Photosubstitution of Ru-complexes with blue light: estimation of reaction half-time

Because the amount of [Ru] inside the cells was unknown, an estimation was based on a 10 µM aqueous solution. The reaction half-time for a prototypical Ru-complex photosubstitution ([Ru-L] + hν → [Ru-H_2O] + L) was estimated using the following set of equations.

$$\frac{dn_{RuOH_2}}{dt} = k \times n_{RuL} \qquad \textit{Equation S VII.1}$$

where n_{RuOH_2} is the amount of Ru-H_2O molecules (mol), n_{RuL} is the amount of Ru-L molecules (mol), and k is the photosubstitution rate, defined by Equation S VII.2:

$$k = W \times \varphi_{454} \times (1 - 10^{-A_{454}}) \times \left(\frac{\varepsilon_{454} \times l}{A_{454} \times V}\right) \times \Phi_{Ru} \qquad \textit{Equation S VII.2}$$

in which W is the surface area of a 96 well-plate well (0.3 cm^2), φ_{454} is the photon flux at 454 nm (7.0 $mW.cm^{-2}$, *i.e.* 2.7 × 10^{-8} $mol.s^{-1}.cm^{-2}$), A_{454} is the absorbance at 454 nm (0.042 for a complex with a molar absorption coefficient (ε_{454}) of 6000 $M^{-1}cm^{-1}$), l is the light path length for a 200 µL work volume (V) in a 96 well-plate well (l = 0.7 cm), and Φ_{Ru} is the photosubstitution quantum yield (usually around 0.01 for such complexes).[3] Under these assumptions, k at t = 0 was estimated to be 3.6 × 10^{-3} s^{-1}. Then, the half time ($t_{1/2}$) of the reaction is given by Equation S VII.3:

$$t_{1/2} = \frac{\ln(2)}{k} \qquad \textit{Equation S VII.3}$$

The value of $t_{1/2}$ was estimated to be 192 s (~ 3 min).

VII.7. UV-vis spectroscopy and mass spectrometry after red-light irradiation of M1-3-6 liposomes

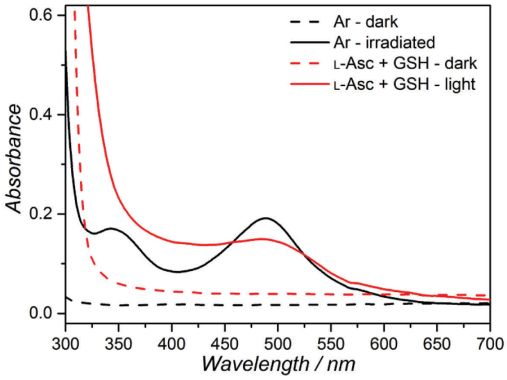


Figure S.VII.9. UV-vis absorption spectra of filtered solutions of red-light irradiated ***M1-3-6*** *liposomes ([DMPC] = 1 mM) under argon (solid black) and in air in presence of 10 mM L-Asc and GSH (solid red). Irradiation was done for 60 min with 2 mL sample volume, 150 mW 630 nm light (1.2 W.cm^{-2} intensity, 4.3 kJ.cm^{-2}), and at 37 °C, and then the solution was filtered with a centrifuge filter (MWCO = 100,000 Da); the UV-vis absorption spectrum of the filtrate is shown here. As controls, samples were kept in the dark and filtered in the same way (dashed lines): these spectra show neither absorption of the upconversion compounds* ***1*** *and* ***3****, nor that of the Ru-complex* ***6***$^{2+}$*, which indicates that no Ru photosubstitution has taken place and that the liposomes remain in the filter.*

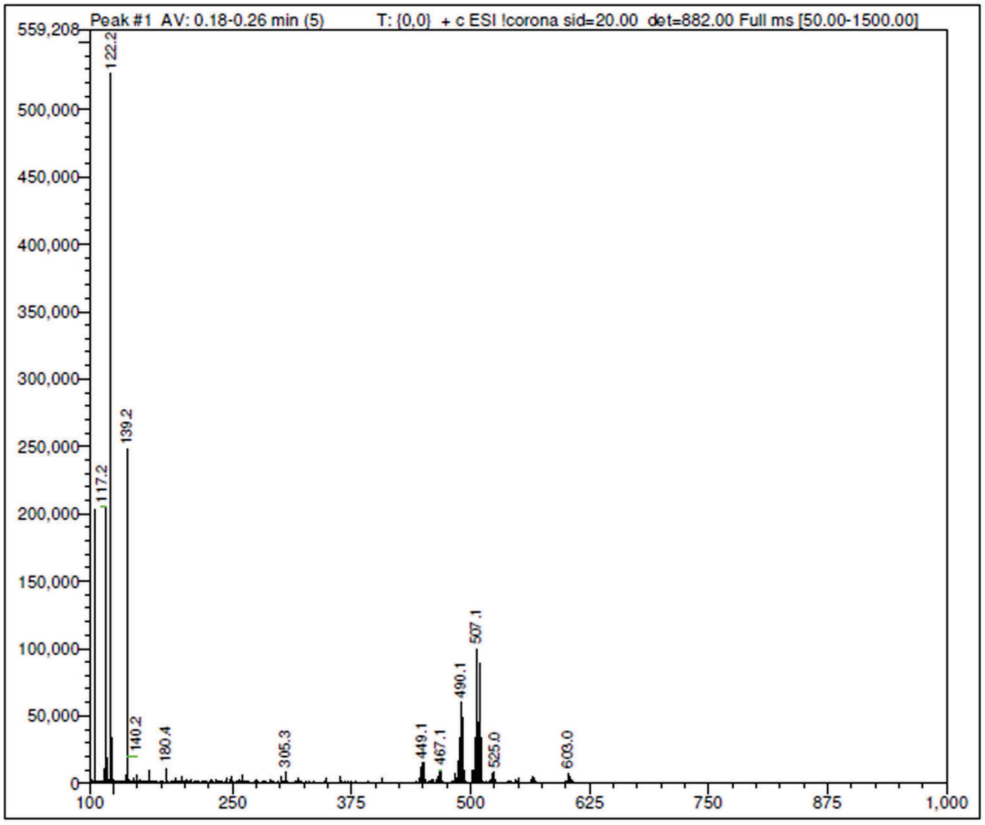


Figure S.VII.10. Mass spectrometry after red light irradiation of ***M1-3-6*** *liposomes (DMPC = 20 mM). After 60 min irradiation with 150 mW 630 nm light (1.2 W.cm⁻²) at 37 °C under argon, the liposome solution was filtered with a centrifuge filter (MWCO = 100,000 Da), the filtrate was lyophilized and redissolved in a minimal amount of acetone. Attribution of main peaks in m/z (calculated): 449.1 $[Ru(bpy)_2Cl]^+$ (449.0); 467.1 $[Ru(bpy)_2Cl(OH_2)]^+$ (467.0); 490.1 $[Ru(bpy)_2(OH_2)(OH)]^+$(MeCN) (490.1); 507.1 $[Ru(bpy)_2(acetone)Cl]^+$ (507.1) or $[Ru(bpy)_2(OH_2)(OH)]^+$(acetone) (507.1).*

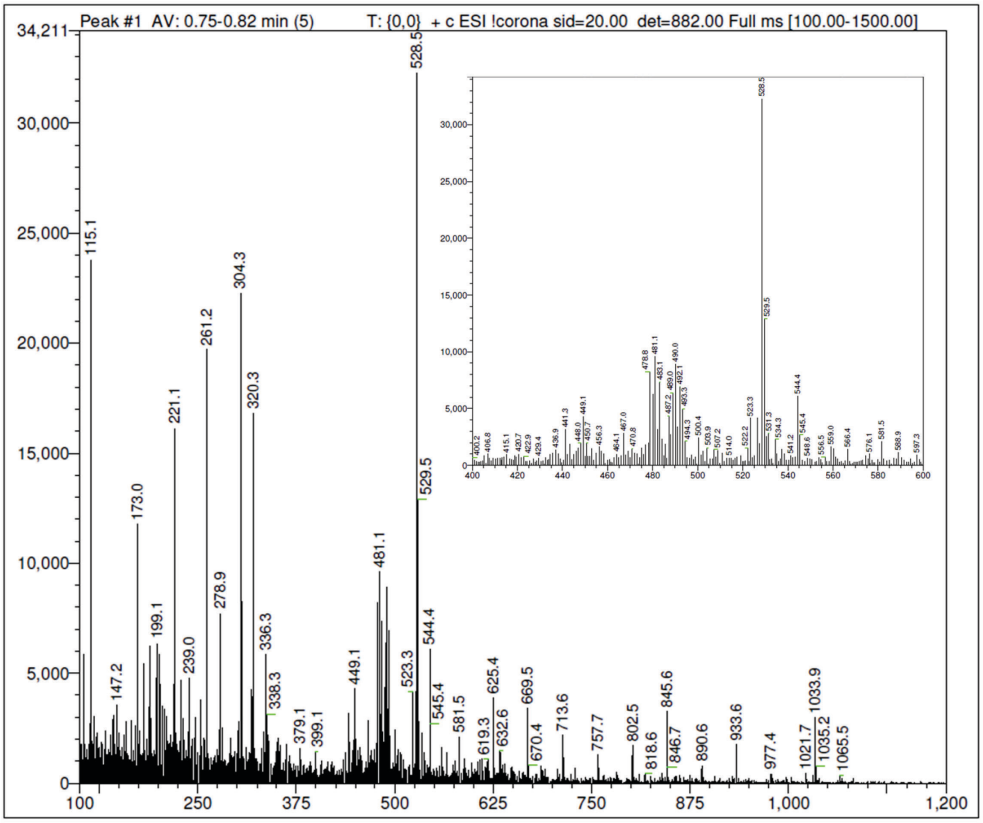


*Figure S.VII.11. Mass spectrometry after red light irradiation of **M1-3-6** liposomes (DMPC = 20 mM) in presence of 10 mM L-Asc and GSH. After 60 min irradiation with 150 mW 630 nm light (1.2 W.cm^{-2}) at 37 °C under argon, the liposome solution was filtered with a centrifuge filter (MWCO = 100,000 Da), the filtrate was lyophilized and redissolved in a minimal amount of methanol. Attribution of main peaks in m/z (calculated): 481.1 [Ru(bpy)$_2$(MeOH)Cl]$^+$ (481.0) or [Ru(bpy)$_2$(OH$_2$)$_2$]$^{2+}$(MeO$^-$) (481.1); 490.0 [Ru(bpy)$_2$(OH$_2$)(OH)]$^+$(MeCN) (490.1). The rest of the signals do not contain a ruthenium isotope pattern.*

VII.8. References

[1] M. Almgren, *J. Am. Chem. Soc.* **1980**, *102*, 7882-7887.

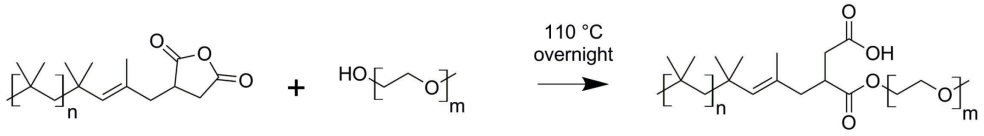
[2] A. Bahreman, B. Limburg, M. A. Siegler, E. Bouwman, S. Bonnet, *Inorg. Chem.* **2013**, *52*, 9456-9469.

[3] A. Bahreman, J.-A. Cuello-Garibo, S. Bonnet, *Dalton Trans.* **2014**, *43*, 4494-4505.

APPENDIX VIII: SUPPORTING INFORMATION FOR CHAPTER 9

VIII.1. Synthesis and characterization of PiB-PEG-Me block copolymers

VIII.1.1. Synthesis



PiB_{1000}-SA PEG_x-Me PiB_{1000}-PEG_x-Me
3: x = 350
4: x = 750

Scheme S.VIII.1. Synthesis of PiB-b-PEG-Me block copolymers 3 and 4 from polyisobutylene succinic anhydride (PiB_{1000}-SA) and mono-methoxy ethylene glycol (PEG_{350}-Me or PEG_{750}-Me).

VIII.1.2. Molecular weights

*Table S.VIII.1. Molecular weights of PiB_{1000}-SA, PEG_{350}-Me, PEG_{750}-Me, and compounds **3** and **4** in weight averaged molecular weight (M_w) and number averaged molecular weight (M_n), according to the manufacturer, gel permeation chromatography (GPC), and NMR, see sections VIII.1.3 and VIII.1.4. Gel permeation chromatography was done in THF with molecular weights reported relative to polybutadiene standards.*

Polymer	**Manufacturer**	**GPC**		**^{1}H NMR**
	M_n (kg.mol^{-1})	M_n (kg.mol^{-1})	PDI (M_w/M_n)	M_n (kg.mol^{-1})
PiB_{1000}-SA	1.05	0.95	1.71	1.11[a]
PEG_{350}-Me	0.35	N/A	N/A	0.36[b]
PEG_{750}-Me	0.75	N/A	N/A	0.80[b]
3	-	1.32	1.50	1.25[b]
4	-	1.18	1.54	2.11[b]

[a] Based on normalization of the alkene signal at 4.6 – 5.3 ppm as 1 proton. [b] Based on normalization of the terminal methyl peak at 3.2 ppm as 3 protons.

For the GPC results, we expected M_n of **4** to have a value in the range of 1.50 to 2.00 kg/mol, but found a value of 1.18 kg/mol. We attribute this to the greater molecular weight of the hydrophilic fraction.

VIII.1.3. Gel Permeation Chromatography (GPC)

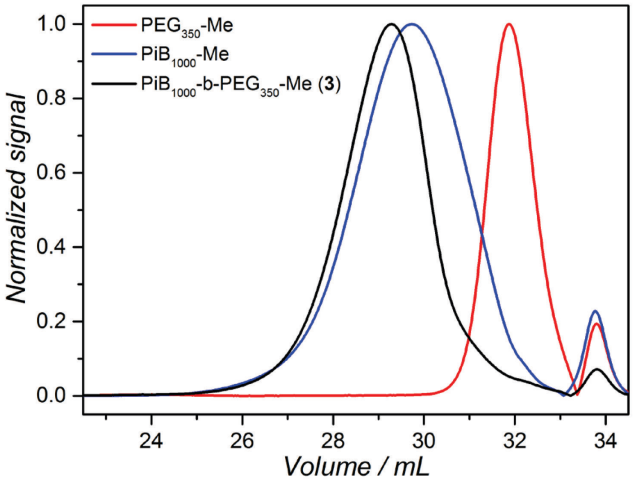


*Figure S.VIII.1. Elugram of monomethyl polyethylene glycol (PEG_{350}-Me, red), polyisobutylene-succinic anhydride (PiB_{1000}-SA, blue), and compound **3** (black).*

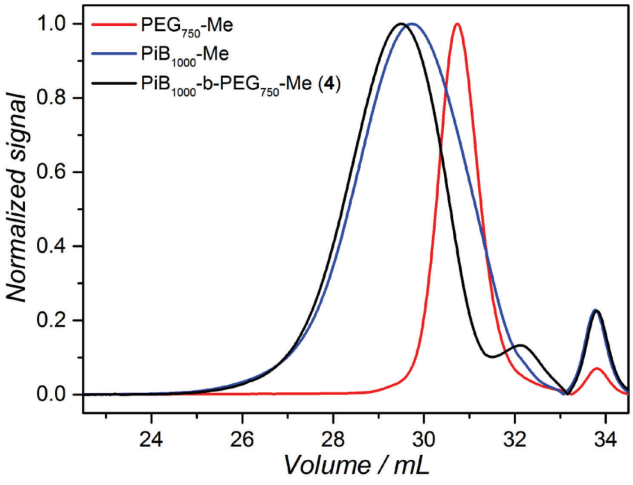


*Figure S.VIII.2. Elugram of monomethyl polyethylene glycol (PEG_{750}-Me, red), polyisobutylene-succinic anhydride (PiB_{1000}-SA, blue), and compound **4** (black).*

VIII.1.4. NMR Spectroscopy

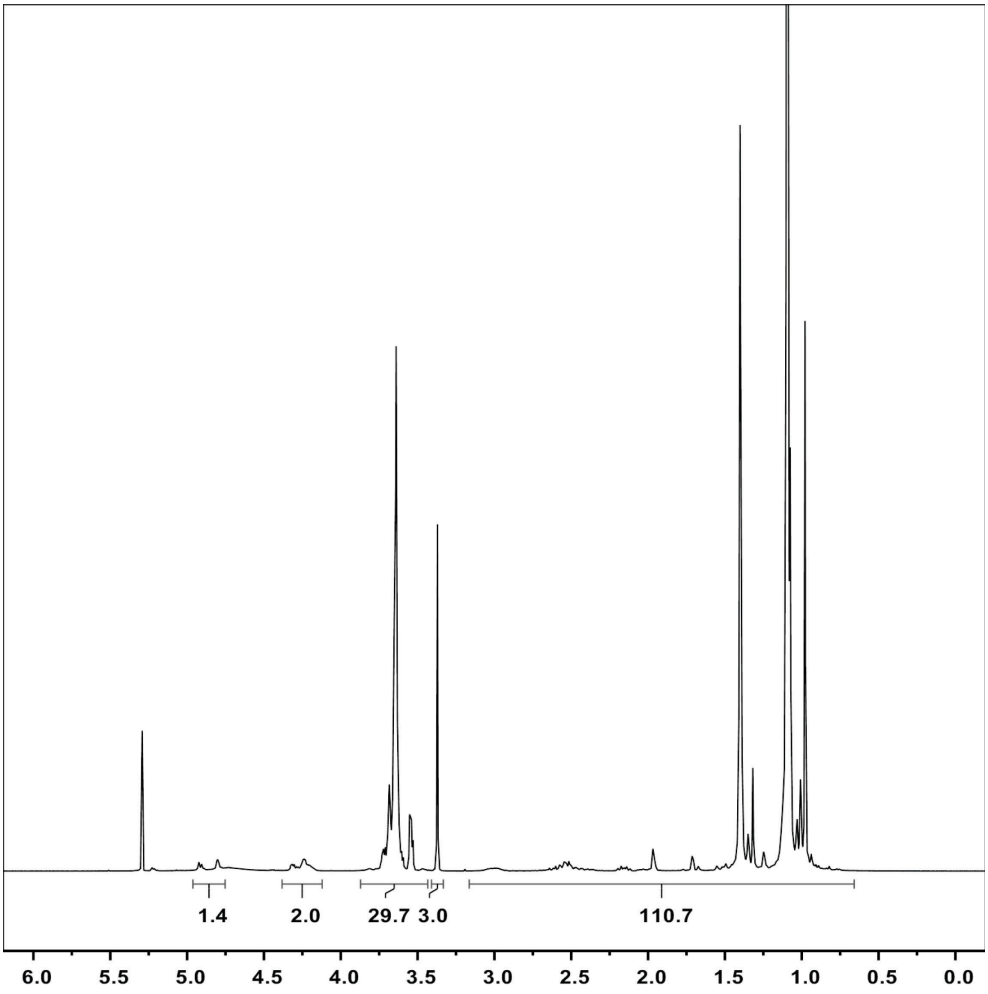


*Figure S.VIII.3. ^{1}H NMR spectrum of compound **3** (PiB_{1000}-b-PEG_{350}-Me) in $CDCl_3$. Attribution: δ (ppm) 4.9 – 4.8 (1 H, C=C of PiB), 4.3 – 4.1 (2 H, alpha protons of the ester), 3.8 – 3.5 (30 H, PEG) 3.4 (3 H, O-CH_3 of PEG-Me), 3.1 – 2.9; 2.8 – 2.4; 2.3 – 2.1; 2.1 – 0.8 (111 H, methyl and methylene of PiB). The spectrum corresponds to literature data.[1]*

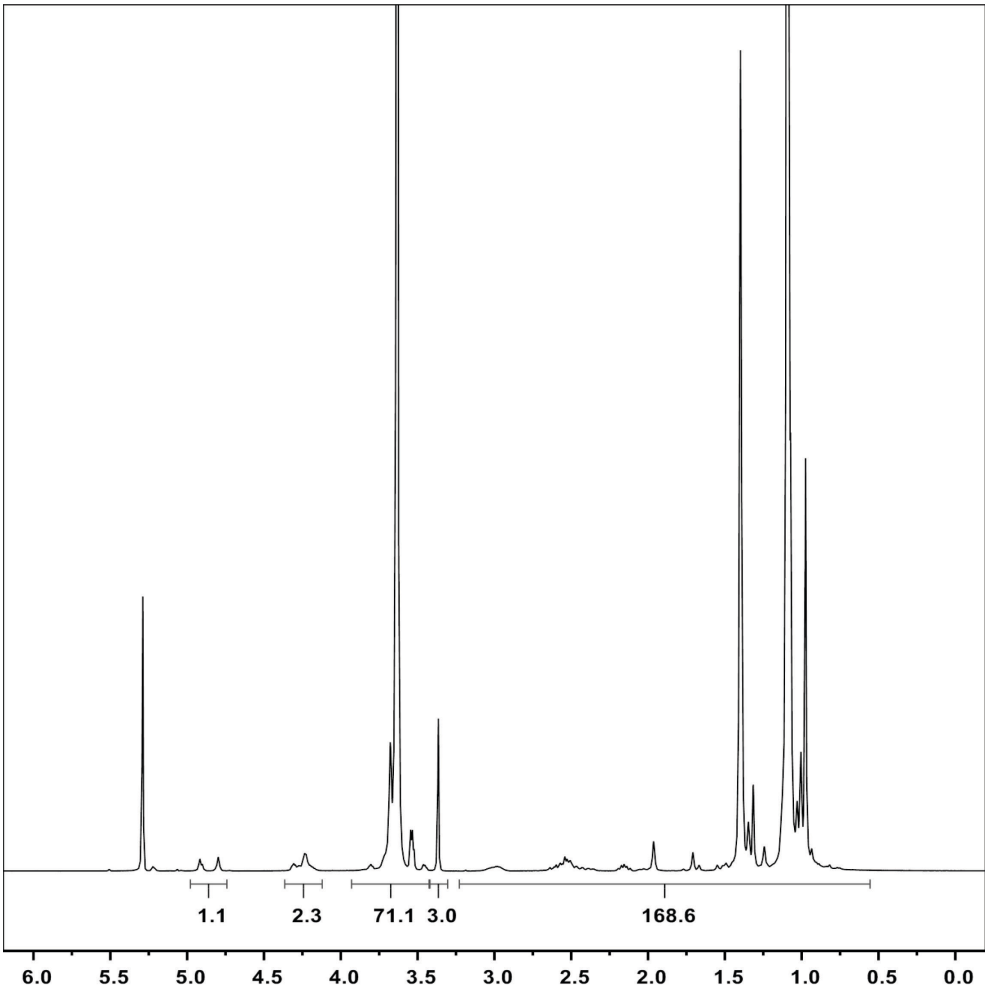


*Figure S.VIII.4. ^{1}H NMR spectrum of compound **4** (PiB_{1000}-b-PEG_{750}-Me) in $CDCl_3$. Attribution: δ (ppm) 4.9 – 4.8 (1 H, C=C of PiB), 4.3 – 4.1 (2 H, alpha protons of the ester), 3.8 – 3.5 (71 H, PEG) 3.4 (3 H, O-CH_3 of PEG-Me), 3.1 – 2.9; 2.8 – 2.4; 2.3 – 2.1; 2.1 – 0.8 (169 H, methyl and methylene of PiB). The spectrum corresponds to literature data.[1]*

VIII.1.5. IR Spectroscopy

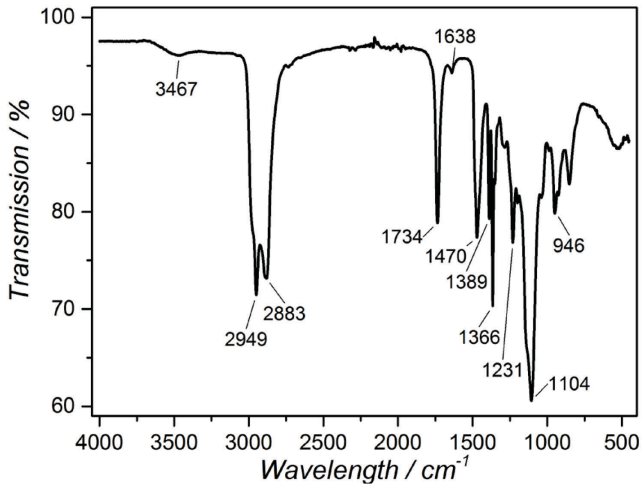


*Figure S.VIII.5. Infrared spectrum of **3** (PiB_{1000}-b-PEG_{350}-Me). Peak assignment (cm^{-1}): 3467 (OH), 2949, 2883 (C-H), 1734 (C=O), 1638 (C=C), 1470, 1389, 1366, 1231 (PiB skeleton), and 1104 (C-O of PEG). The spectrum corresponds to literature data.[1]*

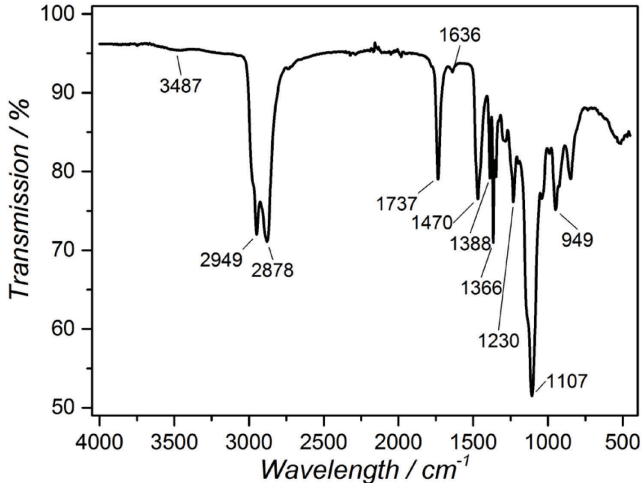


*Figure S.VIII.6. Infrared spectrum of **4** (PiB_{1000}-b-PEG_{750}-Me). Peak assignment (cm^{-1}): 3487 (OH), 2949, 2878 (C-H), 1737 (C=O), 1636 (C=C), 1470, 1388, 1366, 1230 (PiB skeleton), and 1107 (C-O of PEG). The spectrum corresponds to literature data.[1]*

VIII.2. Transmission electron microscopy images of vesicles

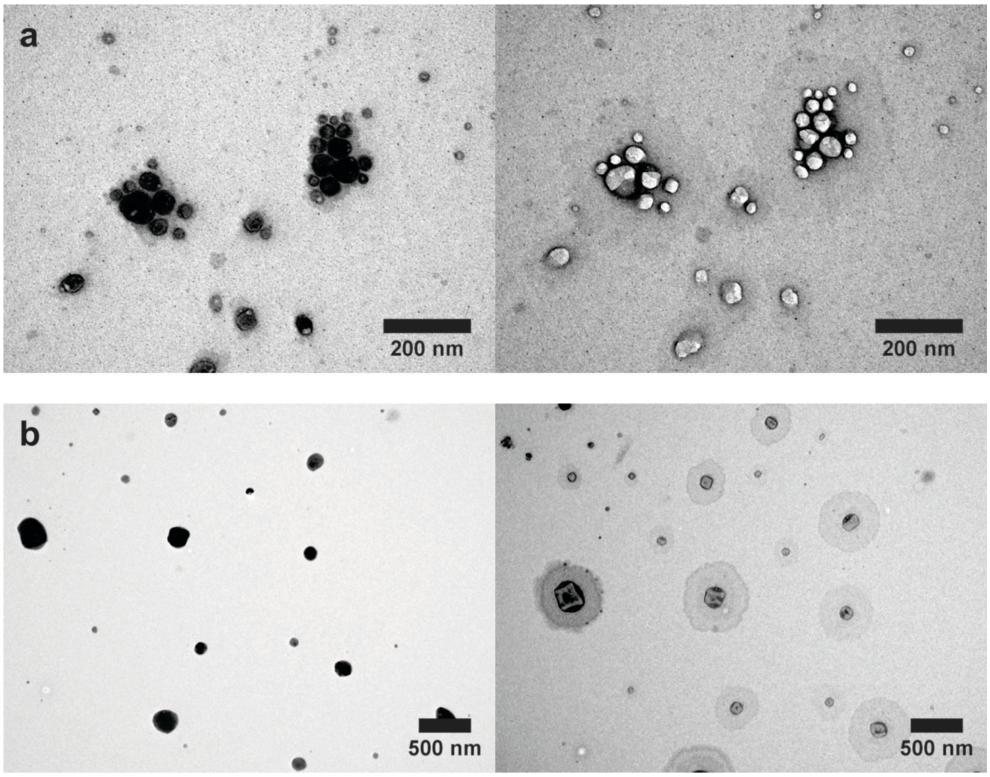


*Figure S.VIII.7. TEM micrographs of **P3** (a) and **P4** (b) vesicles in intact state (left) and after 2 minutes when the vesicles had collapsed and dried out under influence of the electron beam in the transmission electron microscope (right). Note the ring of salt around the vesicles after drying out, indicating the escape of salty water from the vesicles' interior. No TEM-stain was needed to visualize the vesicles.*

VIII.3. Upconversion with 1 and 2 in organic solvent

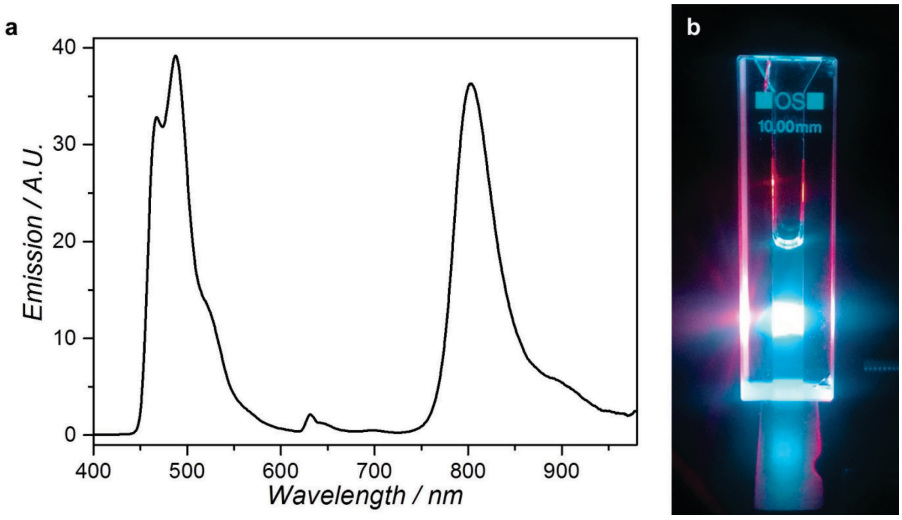


*Figure S.VIII.8. a) Emission spectroscopy of **1** and **2** in a 3:1 v/v chloroform/oleic acid mixture ([**1**] = 7.5 μM, [**2**] = 150 μM) in air, irradiated with 50 mW 630 nm laser light (4 mm beam diameter, 0.4 W.cm^{-2}) in a macro cuvette at 20 °C. No emission filters were used. b) Photograph of the same solution in a semi-micro cuvette, irradiated with a 50 mW 630 nm laser beam (4 mm beam diameter, 0.4 W.cm^{-2}) from the left side. The photograph was taken without filtering the excitation source.*

VIII.4. Compounds 1 and 2 in organic solvent

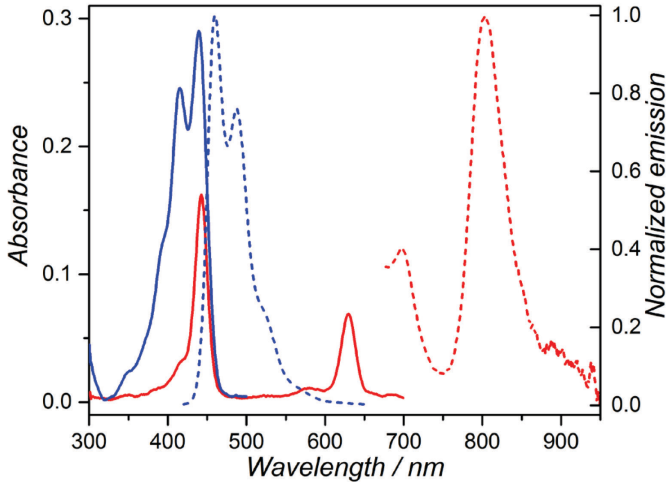


*Figure S.VIII.9. UV-Vis absorbance (solid lines) and emission (dashed lines) spectroscopy of **1** and **2** in chloroform. [**1**] = 0.5 μM, [**2**] = 10 μM. λ_{exc} = 405 nm for compound **2** and λ_{exc} = 630 nm for compound **1**.*

VIII.5. Compounds 1 and 2 in polymersomes

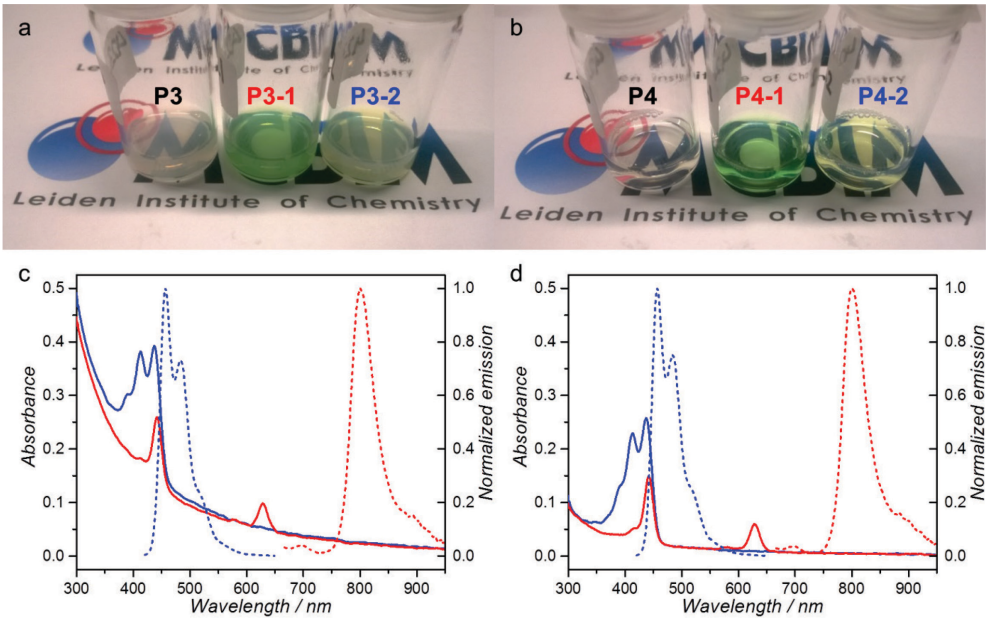


*Figure S.VIII.10. a) Photograph of samples **P3**, **P3-1**, and **P3-2**. b) Photograph of samples **P4**, **P4-1**, and **P4-2**. c) UV-Vis absorbance (solid lines) and normalized emission (dashed lines) of samples **P3-1** (red) and **P3-2** (blue). d) UV-Vis absorbance (solid lines) and normalized emission (dashed lines) of samples **P4-1** (red) and **P4-2** (blue). Conditions: [**3**] = [**4**] = 0.5 mg/mL, [**1**] = 0.5 μM, [**2**] = 10 μM, T = 20 °C, λ_{exc} = 405 nm for **P3-2** and **P4-2** and λ_{exc} = 630 nm for **P3-1** and **P4-1**. Spectra taken in air without anti-oxidants.*

VIII.6. Giant vesicles

To investigate whether TTA-UC truly occurs in the polymer membrane, giant polymersomes with polymer **3** were prepared by following a procedure for self-assembly of phospholipid giant vesicles to make giant polymersomes **GP3-1-2**,[2] and imaged by bright field and emission spectroscopy. First, the vesicles were imaged in a regular fluorescence microscope at 20x magnification and λ_{exc} = 377 nm (Figure S.VIII.11). The bright field images showed microscale spherical vesicles. When excited at 377 nm (*i.e.* direct excitation of **2**), bright fluorescence was observed from the membrane, which proves that **2** was indeed located inside the membrane. Then, the vesicles were imaged with a laser microscopy setup (see experimental section) with 405 and 635 nm excitation in presence of 0.1 M sodium sulfite (Figure S.VIII.12). The addition of the sulfite after GUV preparation caused the vesicles to shrink significantly (compare Figure S.VIII.11 with Figure S.VIII.12), but they could be imaged nonetheless. Again, bright fluorescence was observed

from the membrane when **2** was excited directly (λ_{exc} = 405 nm). The giant vesicles were also illuminated with 635 nm laser light, while selectively imaging between 450 – 575 nm: upconversion emission was indeed detected in the membrane, completely superimposable with the bright field and 405 nm excitation images and ultimately proving that **1** and **2** were co-localized in the polymer membrane. In control experiments, in which **2** was omitted from the formulation (**GP3-1**), only very weak luminescence with 405 nm excitation was observed, due to phosphorescence of **1** at 800 nm that is not entirely blocked with the dichroic mirror and emission filter used for 405 nm excitation. However, no emission was observed with 635 nm excitation, due to strict blocking of everything but 450 – 575 nm. This confirmed that our microscopy setup was indeed selectively imaging upconversion emission under 635 nm excitation.

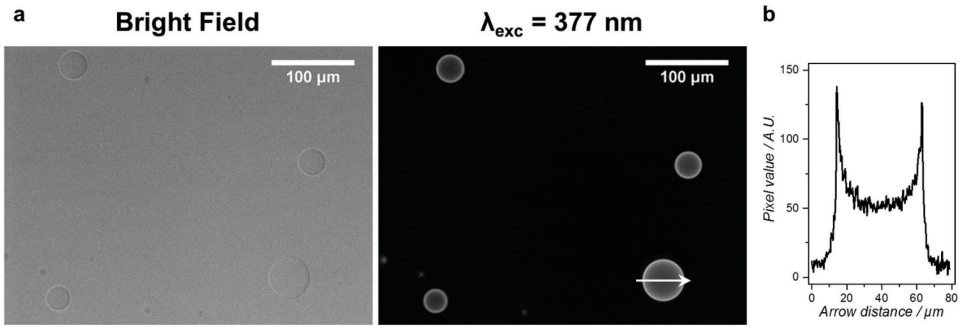


*Figure S.VIII.11. a) Bright field (left) and emission spectroscopy (right, λ_{exc} = 377 nm) of giant polymersomes **GP3-1-2**. The profile plot of the white arrow is given in (b).*

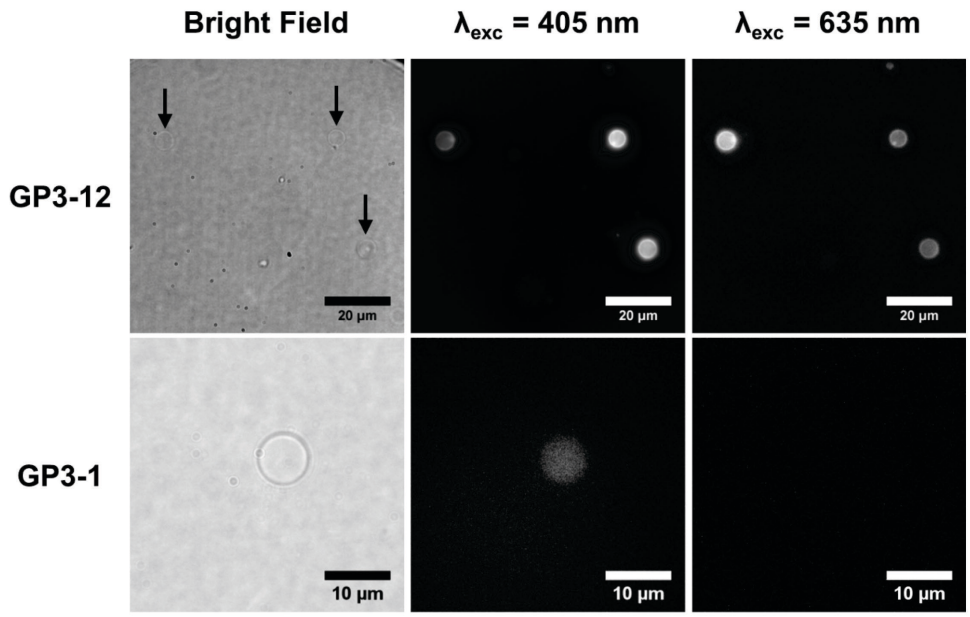


*Figure S.VIII.12. Bright field and emission microscopy images of giant polymersomes **GP3-1-2** (top) and **GP3-1** (bottom). Left: Bright field image. The vesicles are indicated with arrows. Middle: fluorescence microscopy by directly exciting compound **2** with 405 nm light (6.7 µW, 60 µm spot size, intensity 0.24 W.cm^{-2}). Right: upconversion microscopy by exciting compound **1** with 635 nm light (13 mW, 50 µm spot size, intensity 640 W.cm^{-2}) and imaging from 450 to 575 nm. The images were acquired in air in presence of 0.1 M Na_2SO_3.*

VIII.7. Temperature dependency of TTA-UC in polymersomes

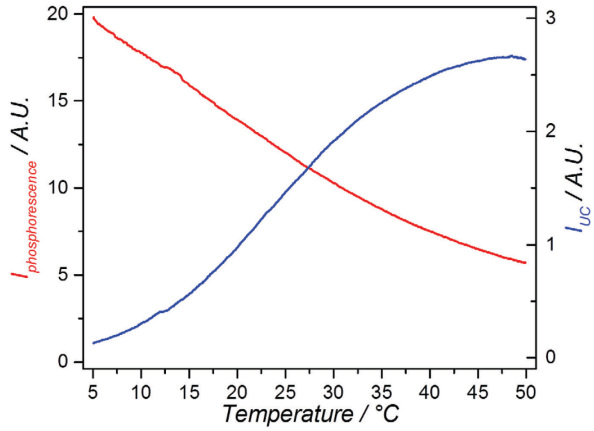


*Figure S.VIII.13. Temperature dependency of phosphorescence (red) and upconversion emission (blue) in **P4-1-2** vesicles (0.5 mg/mL compound **4**) irradiated with 50 mW 630 nm (4 mm diameter, 0.4 W.cm^{-2}) in presence of 50 mM sodium sulfite. Experiment with **P3-1-2** vesicles yielded very similar results.*

VIII.8. Power dependency of TTA-UC in polymersomes

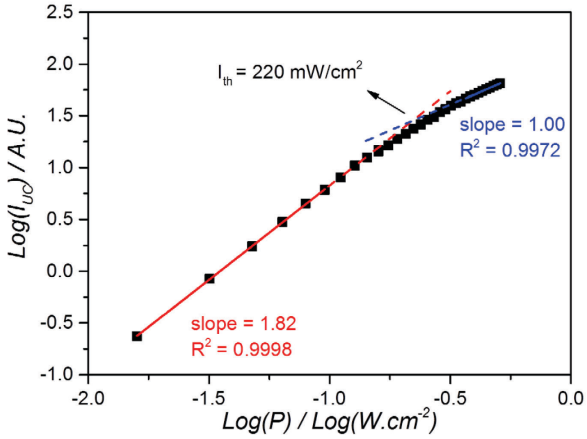


*Figure S.VIII.14. Power dependency of upconversion emission in **P4-1-2** vesicles (0.5 mg/mL compound **4**) at 20 °C. The red and blue lines are straight fit curves through the first and last data points, respectively, where the intersection of the two lines represent the intensity threshold (I_{th}). Experiment with **P4-1-2** at 37 °C, and experiments with **P3-1-2** at 20 °C and 37 °C yielded very similar results.*

VIII.9. Time evolution of upconversion with P3-1-2 and P4-1-2 in air and dye bleaching

VIII.9.1. P3-1-2 vesicles

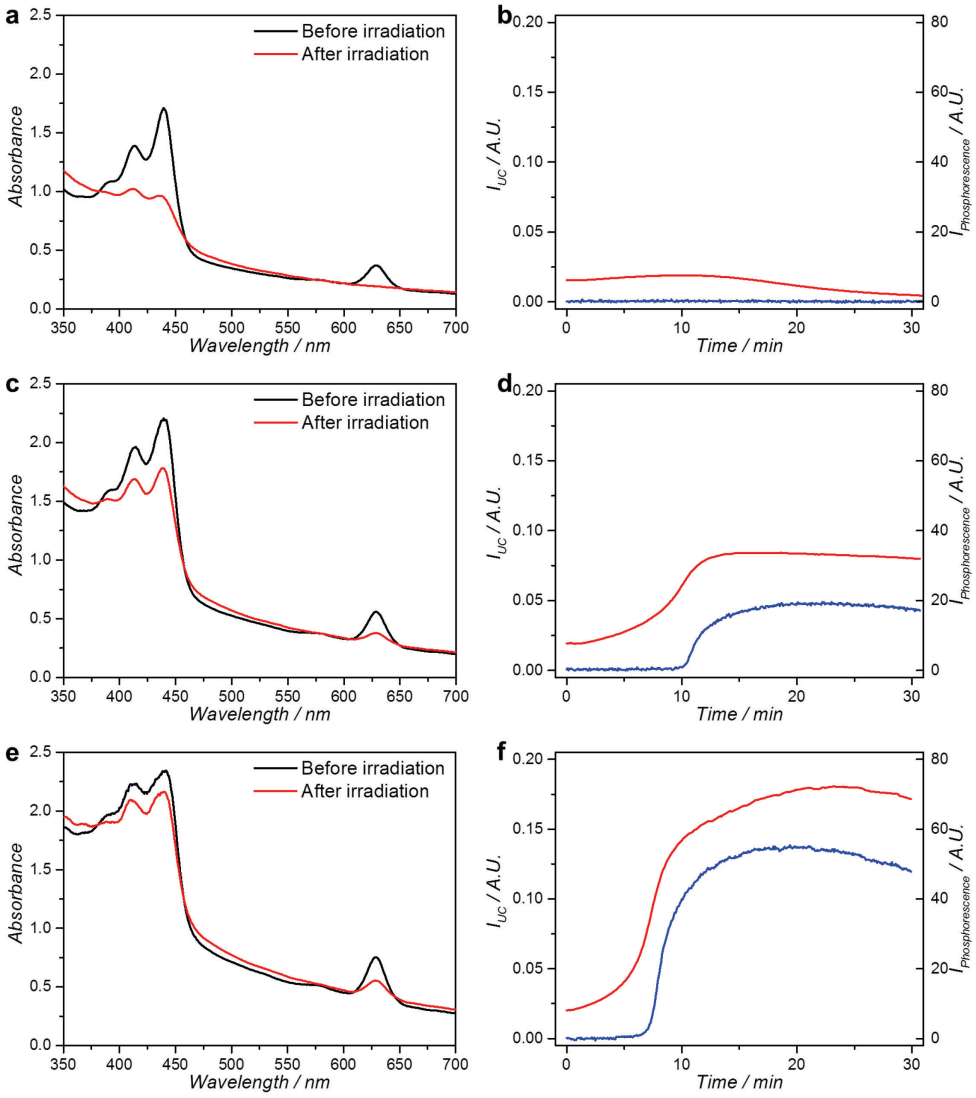


*Figure S.VIII.15. Red-light irradiation of **P3-1-2** vesicles at 5.0 (a, b), 7.5 (c, d), and 10 mg/mL (e, f) in air and in absence of added oxygen-scavenger. UV-Vis absorption spectra (a, c, e, 4 mm path length) before (black) and after (red) 30 min 630 nm irradiation (50 mW, 0.4 W.cm^{-2}, 4 mm path length) showing dye bleaching. Emission time traces (b, d, f) during the irradiation experiment, showing I_{UC} (blue, left axis) and $I_{phosphorescence}$ (red, right axis). Conditions: 600 µL sample in a semi-micro cuvette at 20 °C.*

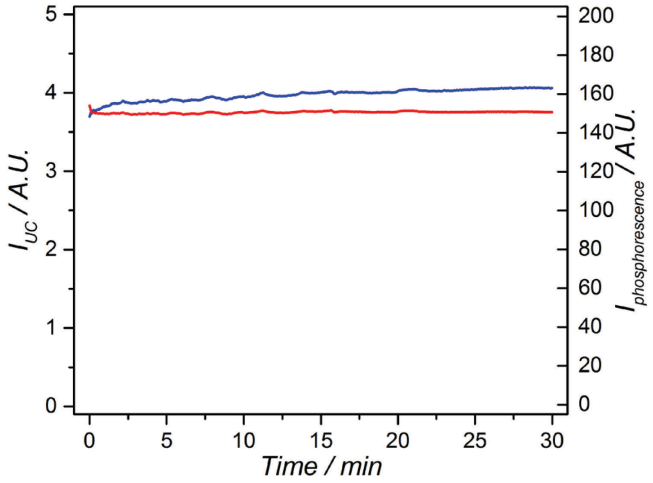


Figure S.VIII.16. Emission time traces of a 7.5 mg/mL ***P3-1-2*** *sample with addition of 75 mM* Na_2SO_3 *as oxygen scavenger, showing* I_{UC} *(blue, left axis) and* $I_{phosphorescence}$ *(red, right axis), during 50 mW 630 nm (0.4 W.cm*$^{-2}$*, 4 mm path length) irradiation.*

VIII.9.2. P4-1-2 vesicles

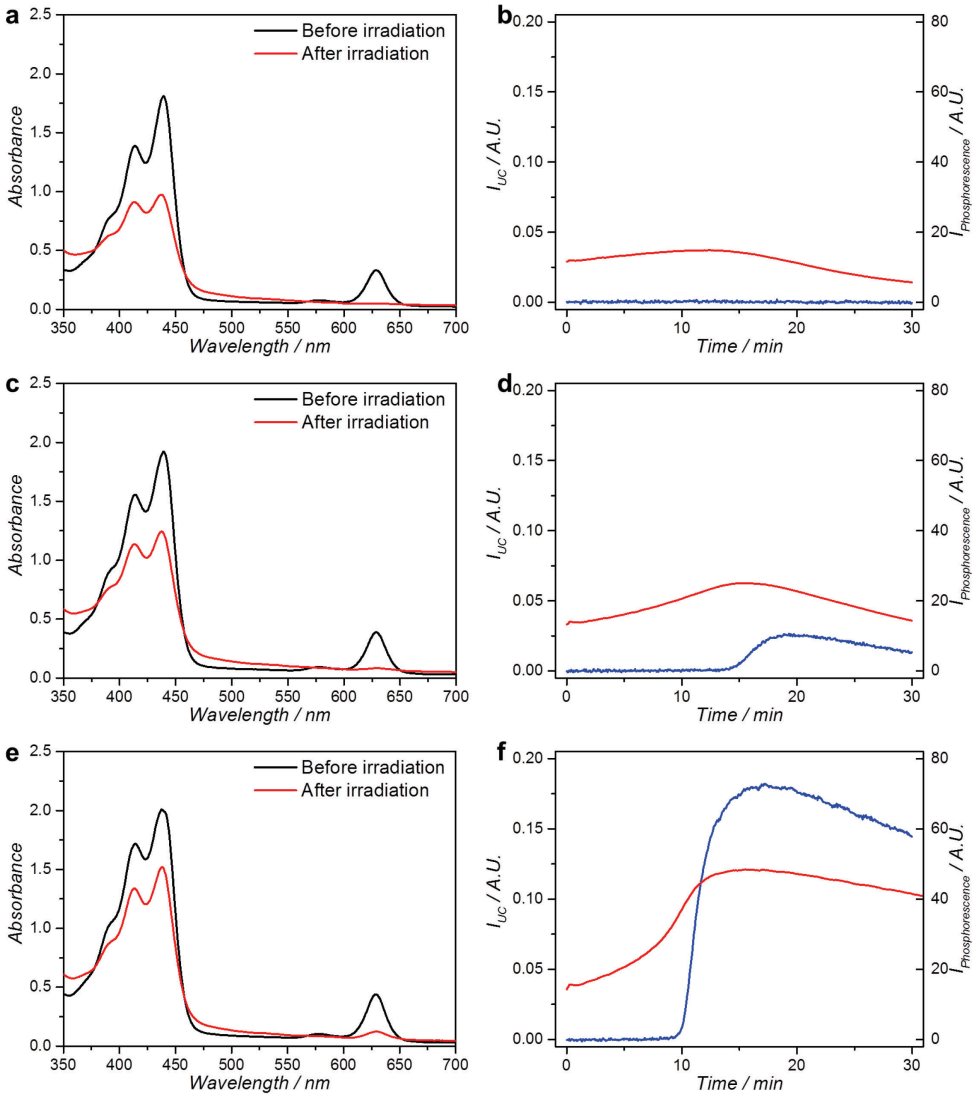


*Figure S.VIII.17. Red light irradiation experiments with **P4-1-2** vesicles at 7.5 (a, b), 8.8 (c, d), and 10 mg/mL (e, f) in air without added anti-oxidants. UV-Vis absorption spectra (a, c, e, 4 mm path length) before (black) and after (red) 30 min 630 nm irradiation (50 mW, 0.4 W.cm^{-2}, 4 mm path length) showing bleaching. Emission time traces (b, d, f) during the irradiation experiment, showing I_{UC} (blue, left axis) and $I_{phosphorescence}$ (red, right axis). Conditions: 600 µL sample in a semi-micro cuvette at 20 °C.*

VIII.10. Oxygen consumption during red light irradiation of P3-1-2 and P4-1-2 in air

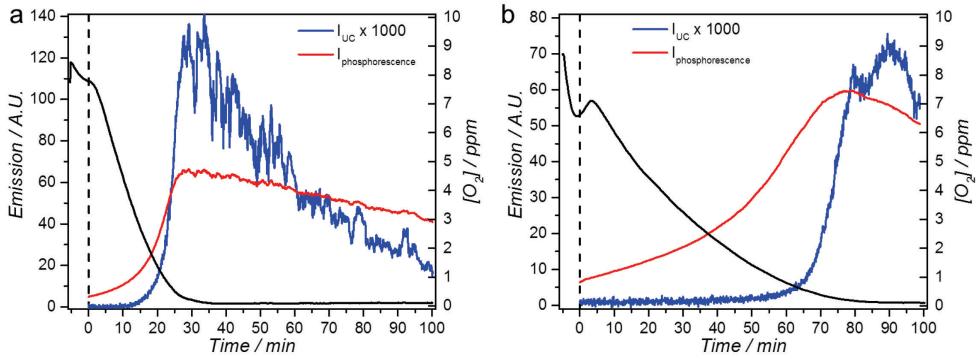


*Figure S.VIII.18. Upconversion intensity I_{UC} (blue, data multiplied by 1000 for clarity, left axis), phosphorescence intensity $I_{phosphorescence}$ (red, left axis), and dissolved oxygen concentration (black, right axis, measured using a submerged oxygen probe) during 50 mW 630 nm light irradiation (10 mm path length, 4 mm beam diameter, 0.4 W.cm^{-2}) of 2.0 mL samples of **P3-1-2** (a) or **P4-1-2** (b) at 10 mg/mL polymer concentration in a stirred macro cuvette at 20 °C. Laser was turned on at t = 0, as indicated by the dashed line, and I_{UC} and $I_{phosphorescence}$ were recorded at 486 and 800 nm, respectively.*

VIII.11. Oxygen and emission time traces of diluted samples of P4-1-2 without addition of oxygen scavengers

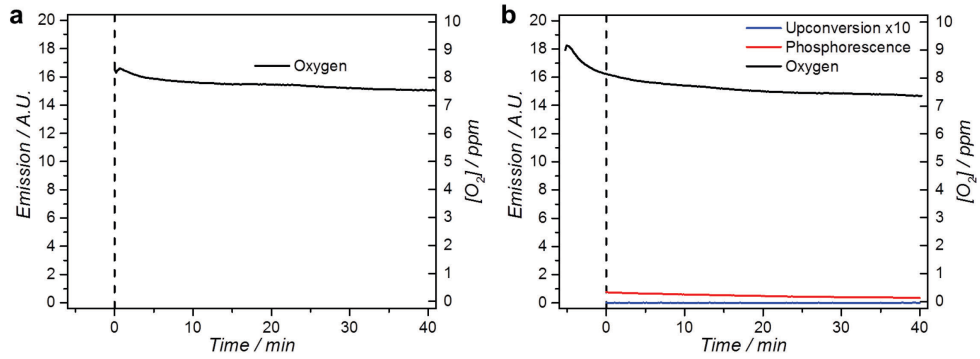


*Figure S.VIII.19. Oxygen measurement of a **P4-1-2** sample without the addition of oxygen scavengers in the dark (left) and during 50 mW 630 nm (0.4 W.cm^{-2}) excitation (right). Red and blue line represent photosensitizer phosphorescence at 800 nm and upconversion emission at 486 nm, respectively. **[4]** = 0.5 mg/mL, **[1]** = 0.5 µM, **[2]** = 10 µM, T = 20 °C, 2 mL sample volume in a stirred macro cuvette. Laser was turned on at t = 0, as indicated by the dashed line.*

VIII.12. Cell imaging with upconverting polymersomes

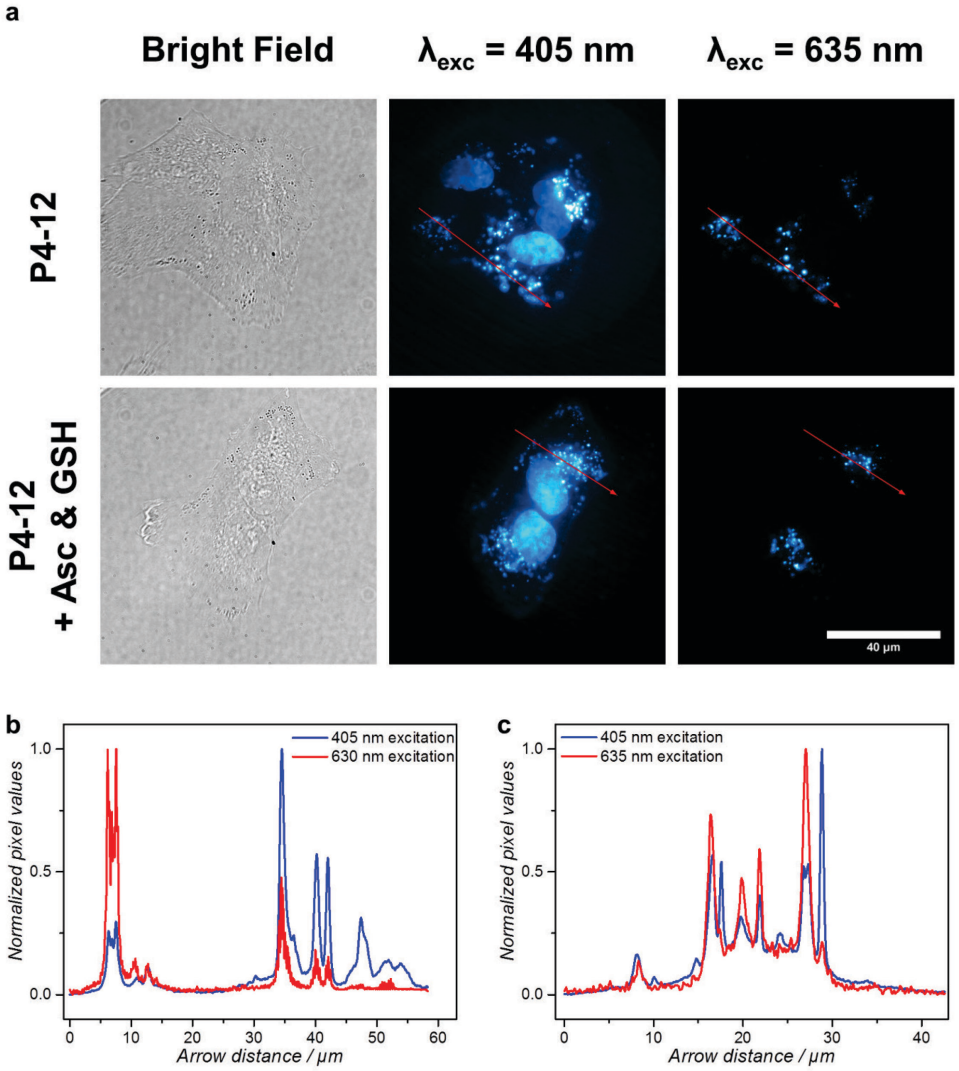


*Figure S.VIII.20. a) Imaging of **P4-1-2** upconverting polymersomes in A549 lung carcinoma cells in bright field mode (left column), with λ_{exc} = 405 nm (middle column), and with λ_{exc} = 635 nm (right column). Cells were incubated for 4 h with 1:1 v/v mixture of Opti-MEM and **P4-1-2** vesicles (top row, [**4**] = 0.5 mg/mL), or with 1:1 v/v mixture of Opti-MEM and **P4-1-2** vesicles ([**4**] = 0.5 mg/mL) and addition of 5 mM sodium L-ascorbate and 5 mM sodium glutathionate (bottom row). The cell nuclei were stained with Hoechst 33342 prior to imaging (1 µg/mL in PBS, incubated for 20 min). Imaging conditions: T = 37 °C, 7.0% CO_2, 1.0% O_2, 62 µW 405 nm laser power (60 µm spot diameter, 2.2 W.cm^{-2} intensity), 13 mW 635 nm laser power (50 µm spot diameter, 640 W.cm^{-2} intensity), cells were allowed to equilibrate for 30 min before imaging. b/c) Profile plots of the red arrows in panel [a] in absence (b) or presence (c) of sodium L-ascorbate and sodium glutathionate, with 405 nm (blue line) or 635 nm excitation (red line).*

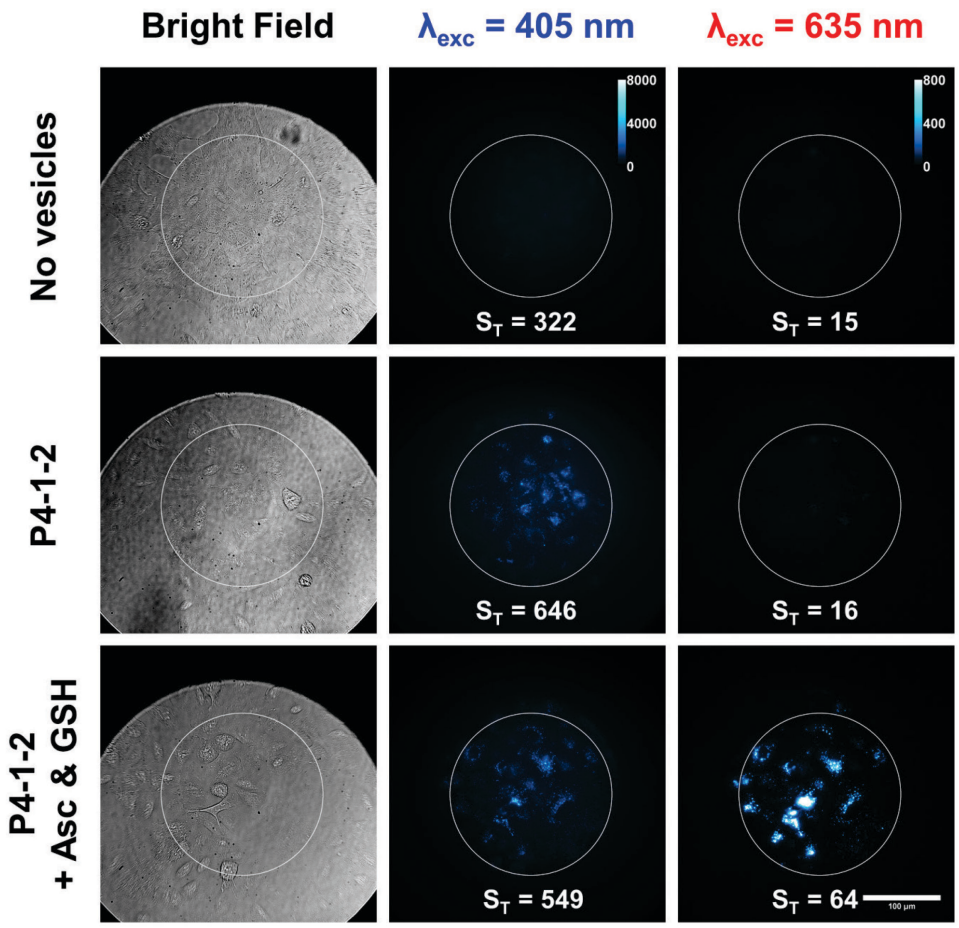


Figure S.VIII.21. Example images used for quantification of in vitro upconversion luminescence. Imaging of ***P4-1-2*** *upconverting polymersomes in A549 lung carcinoma cells in bright field mode (left column), with* λ_{exc} *= 405 nm (middle column), and with* λ_{exc} *= 635 nm (right column) with 40x magnification. Cells were incubated for 4 h with Opti-MEM only (top row),with 1:1 v/v mixture of Opti-MEM and* ***P4-1-2*** *vesicles (middle row, [4] = 0.5 mg/mL), or with 1:1 v/v mixture of Opti-MEM and* ***P4-1-2*** *vesicles ([**4**] = 0.5 mg/mL) and addition of 5 mM sodium L-ascorbate and 5 mM sodium glutathionate (bottom row). Imaging conditions: T = 37 °C, 7.0%* CO_2*, 1.0%* O_2*, 76 µW 405 nm laser power (150 µm spot diameter, 0.44* $W.cm^{-2}$ *intensity), 13 mW 635 nm laser power (131 µm spot diameter, 97* $W.cm^{-2}$ *intensity), cells were allowed to equilibrate for 30 min before imaging. For comparison, the image histograms for* λ_{exc} *= 405 nm are scaled from 0 – 8000 pixel values, and for* λ_{exc} *= 635 nm are scaled from 0 – 800 pixel values, as given by the calibration bars in the top row. In each image, the region of interest (ROI) is indicated with a white circle, and the total signal* S_T *(in mean pixel value) within the ROI is given.*

VIII.13. Emission spectroscopy setup

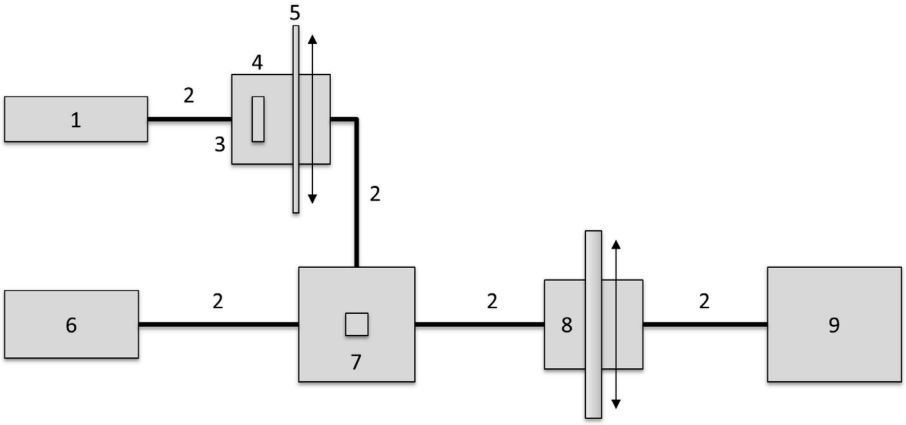


Figure S.VIII.22. Setup used for photosubstitution experiments using red light. Legend: (1) 630 nm laser source, (2) optical fibers, (3) filter holder, (4) 630 nm band pass filter, (5) variable neutral density filter that can be installed or removed, (6) halogen-deuterium light source for UV-Vis absorption spectroscopy, (7) temperature controlled cuvette holder, (8) variable filter holder, and (9) CCD spectrometer.

VIII.14. References

[1] U. Karl, C. Sierakowski, M. Darijo, M. Haberer, H. Hartl, Use Of Amphiphilic Block Copolymers For Producing Polymer Blends, **2008**, 20080293886

[2] a) S. H. C. Askes, N. Lopez Mora, R. Harkes, R. I. Koning, B. Koster, T. Schmidt, A. Kros, S. Bonnet, *Chem. Commun.* **2015**, *51*, 9137-9140; b) N. Lopez Mora, J. S. Hansen, Y. Gao, A. A. Ronald, R. Kieltyka, N. Malmstadt, A. Kros, *Chem. Commun.* **2014**, *50*, 1953-1955.